Biosensors and Bioelectronics 130 (2019) 397–407

Contents lists available at ScienceDirect

Biosensors and Bioelectronics

journal homepage: www.elsevier.com/locate/bios

Protein microarray spots are modulated by patterning method, surface chemistry and processing conditions

Kathryn F.A. Clancy[a,b], Sebastien Dery[b], Veronique Laforte[b,c,d], Prasad Shetty[a], David Juncker[b,d,*], Dan V. Nicolau[a,*]

[a] Department of Bioengineering, McGill University, Montreal, Canada
[b] Department of Biomedical Engineering, McGill University, Montreal, Canada
[c] Department of Neurology and Neurosurgery, McGill University, Montreal, Canada
[d] McGill University and Génome Québec Innovation Center, Montreal, Canada

ARTICLE INFO

Keywords:
Protein microarray
Inkjet printing
Pin printing
Micro-contact printing
Microarray spot

ABSTRACT

The uniformity of the protein patterns, their shape, and the contrast between the fluorescence signal of the pattern and the background, critically modulate the quantitative accuracy of the microarray-derived data. While significant research focused of the identification of the factors that impact the protein microarray patterns, these studies usually have focused on the optimization of one set of these factors, e.g., how the spot uniformity is affected by different additives, or by different surfaces. However, the complex interaction between proteins, carrier fluids, surfaces, and patterning methodologies used would suggest a systematic and more comprehensive study that considers all these parameters, as well as their inter-relationship. The present work compared the patterning of two fluorescently-tagged proteins, i.e., IgG, BSA, on surfaces with different hydrophobicity and chemistry, and printed by inkjet, pin, and microcontact printing (μCP). The quantification of the spot size regularity, its morphology, the signal intensity and its distribution within spots were used to assess the quality of a specific printing method, on a specific surface, with a specific solute of the printed protein. It was found that the optimal uniformity for both droplet-based methods depend on surface chemistry, with glass slides modified with 3-Glycidoxypropyl-dimethoxymethyl silane (GPS) and 3-(Aminopropyl)-triethoxy silane (APTES) exhibiting the greatest uniformity, while uniformity of the μCP patterns was relatively independent of the surface chemistry. For the inkjet and pin printing, the largest fluorescence signal and contrast with the background was found on APTES modified glass slides, whereas for the μCP the fluorescence signal increased with increasing hydrophilicity.

1. Introduction

Microarrays are widely-used analytical tools for drug discovery (Kumble, 2007), biomarker detection (Lee et al., 2008), and diagnosis (Babel et al., 2009; Harwanegg and Hiller, 2005). Owing to the critical role of proteins in physiological processes and health conditions, coupled with the emergence of alternative methods for sequencing DNA not available for proteins protein-based microarrays constitute an attractive technology for protein quantification (Anderson et al., 2011; Bergeron et al., 2015; Müller and Nicolau, 2005). While microarray technology is, arguably, its largest 'market', protein patterning was used for several decades for various applications, in particular for cell engineering, e.g., stem cell constructs (Deforest and Tirrell, 2015), immunoaffinity-based circulating tumor cell capture (Launiere et al., 2012), neuronal cell networks (Nicolau et al., 1999b), but also for on chip enzyme microreactors (Qu et al., 2004), controlling the motion of cytoskeletal filaments on molecular motor tracks (Nicolau et al., 1999a) and for the analysis of protein-analyte interactions (Ricoult et al., 2014; Romanov et al., 2014). Despite this large variety of applications, and despite the wide range of technologies available, finding the optimum conditions for protein patterning still requires extensive experimentation (Vasina et al., 2009), largely due to the very complex interaction of proteins with surfaces (Hanson et al., 2017).

For protein microarrays, the appropriate parameters of the primary protein layer, i.e., consistent spot size, uniformity within and between spots, and morphology (Barbulovic-Nad et al., 2006) are critical to enable an efficient and uniform binding of the secondary analyte, which in turn results in a correct readout and high quality of microarray data.

* Corresponding authors.
E-mail addresses: david.juncker@mcgill.ca (D. Juncker), dan.nicolau@mcgill.ca (D.V. Nicolau).

https://doi.org/10.1016/j.bios.2018.09.027
Received 30 June 2018; Received in revised form 5 September 2018; Accepted 6 September 2018
Available online 07 September 2018
0956-5663/

To improve its performance, which depends on the minimization of the variability of technological parameters, microarray technology, a high throughput technology par excellence, relied on an ever-increasing automation and standardization, and on image analysis based on (i) the output patterned spots adhering to the expected size and morphology, and (ii) their reproducibility. However, these advances in robotics and scanner precision, which led to a large increase in the throughput of microarray data, cannot by themselves address the sheer complexity and multitude of the physical and chemical processes involved that lead to still noisy and imprecise microarray data (Moran-Mirabal et al., 2007; Saeed et al., 2003). Indeed, the many interrelated input parameters e.g., the deposition technique, the surface chemistry and hydrophobicity of the substrate, the physico-chemical properties of the carrier fluid, the drying process, the microenvironment, which all modulate the spot size, morphology and uniformity, also add to the inherent complexity of protein interactions with surfaces (Angulo, 2008; Askounis et al., 2015; Austin and Holway, 2011a; Barbulovic-Nad et al., 2006; Bergeron et al., 2015; Cui et al., 2012; Dufva, 2005; Ivanova et al., 2006; Moran-Mirabal et al., 2007; Mujawar et al., 2014, 2013, 2012; Yunker et al., 2011). In a previous protein microarray study systematically evaluating different buffer and slide chemistries, it was found that the analyte binding signal was tightly correlated to the of signal of antibody (IgG) deposited on the surface (Bergeron, 2015), indicating that the protein binding signal can serve as a proxy for microarray performance.

To this end, we investigated how the deposition method, i.e., physical transfer to the target surface using pin, inkjet and microcontact printing, the properties of the carrier fluid, i.e., various compositions of the buffers and wash solutions, the properties of the immobilizing surface, i.e., chemistry, contact angle, as well as the nature of the protein, i.e., IgG and BSA, affect the quality of the resulting primary protein pattern inferred from the spatial distribution of fluorescence signal. The parameters compared in this work include the size and morphology of the resulting spot, as well as signal intensity and the spatial distribution of protein, i.e., uniformity, within a microarray spot.

2. Materials and methods

2.1. Reagents

A standard phosphate buffered saline (PBS) solution was used as a diluent for all printing methods. Additionally, a PBS solution with 2,3-butanediol/2 M betaine (PBSbb) was used with the inkjet and pin printing methods. The concentrations of additives in the printing buffers have been described elsewhere (Bergeron et al., 2015).

2.2. Proteins

Purified fluorophore-conjugated IgG (Cy5 Goat Anti-Rabbit IgG (H +L), from Life Technologies), and fluorophore-conjugated BSA (Alexa Fluor® 647), from Molecular Probes have been used for protein microrarays.

2.3. Surfaces

Glass slides (Fisher Scientific) were functionalized with 3-Glycidoxypropyl-dimethoxymethyl silane (GPS), Trichloro(octyl) silane (OTS), 3-(Aminopropyl)-triethoxy silane (APTES), and Trichloro (1H,1H,2 H,2H-perfluorooctyl) silane (PFS). Glass slides have been also treated by plasma to produce hydrophilic glass surfaces (P).

Contact angles were measured with a goniometer (OCA 15 EC, Dataphysics).

2.4. Inkjet printing

A non-contact piezo-microarrayer (Nanoplotter 2.0, GeSiM) with a single nozzle was used to deposit 0.4 nL of protein solution on target surfaces to create 8 × 8 arrays with a pitch of 200 μm between spots, for a total of 16 spots per concentration, per replicate slide (Supplementary Figure SI 1). All printing was performed at room temperature and 65% humidity.

2.5. Pin printing

Contact pin printing used a customized Nanoplotter 2.1 microarrayer (GeSiM, Germany) equipped with collimator (Parallel Synthesis, Santa Clara, CA). Four custome made silicon quill pins (Laforte et al., 2013) were used simultaneously to create 5 × 5 arrays of replicate 63–74 pL spots with a pitch of 200 μm for a total of 100 spots per concentration, per replicate slide (Supplementary Figure SI 1).

2.6. Micro-contact printing (μCP)

A patterned silicon wafer was used to fabricate flat, 15 μm-wide square masters with a pitch of 75 μm between square posts. Poly(dimethylsiloxane) (PDMS) stamps (Supplementary Figure SI 4) replicating the masters were inked with 10 μl of the fluorophore conjugated protein solution, rinsed, dried and then used for printing by placing a 25 mg weight placed on top.

2.7. Image acquisition and analysis

Fluorescent images were obtained using an Agilent G2565CA microarray scanner at a 2 μm x 2 μm resolution. The raw image files were first segmented based on predefined search areas, then automatic thresholding was performed, and the spots outside of the expected area were eliminated.

The cross-section of the fluorescence signal across a spot was quantified (Fig. 1A) by estimating a ‘‘coffee-ring’ ratio’, CRR (Fig. 1B), i.e., the ratio between the number of pixels found in the outer 50% of the spot vs. the number of pixels within the inner 50% of the spot. CRR values of −1, 0 and + 1, represents the ‘coffee-ring’ morphology, a perfectly even distribution of the fluorescent pixels within the spot, and the ‘bull's eye’ morphology, respectively (Supplementary Information, Glossary).

A comprehensive description of the methods and materials used is provided in the Supplementary Information section.

3. Results and discussion

3.1. Microarray deposition techniques

While a multitude of deposition technologies have been proposed for the fabrication of microarrays, e.g., pin printing (Austin and Holway, 2011b), ink jet printing (McWilliam et al., 2011), microcontact printing (Renault et al., 2002), electrospray deposition (Avseenko et al., 2002), laser ablation (Ivanova et al., 2002; Nicolau et al., 2010), arguably only the pin and jet printing technologies have received wide spread usage in the fabrication of high throughput microarrays, due to their technological simplicity and capacity for automation.

Indeed, pin printing, which was the pioneer microarray technology (Schena et al., 1995), and which even led to a very high density protein printing based on Atomic Force Microscopy (Lee et al., 2004) relies on the contact between a pin, wetted with the analyte solution, and the target surface. The delivery of a solution by pin printing is based on capillary forces (Štulík, 2011). The advantages of pin printing are its simplicity, and the spatial precision for the spot deposition, while its disadvantages are the contact, at times deleterious, between the pin and the substrate, and the complex process of transfer of the fluid from the

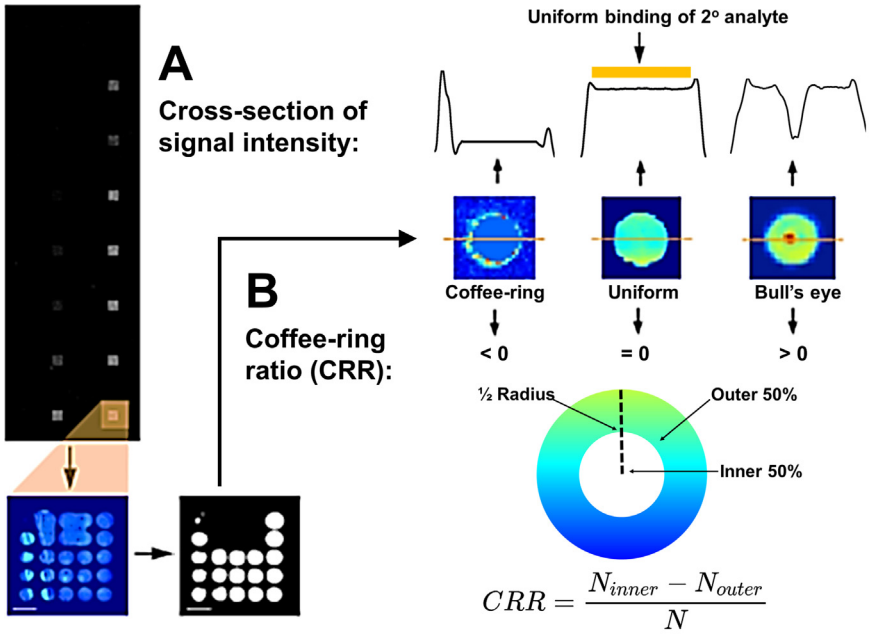

Fig. 1. Conceptual illustration of the image acquisition analysis and the parameters quantifying the protein deposition within a spot. A. The analysis focuses on a set of microarray spots with digitized intensities able to measure the fluorescence intensity profile across the spot. Scale bars are 200 μm. B. Calculation methodology for 'coffee-ring' ratio, from various intensity profiles across the spot, from the coffee-ring, to bull's eye pattern, respectively. The spatially uniform distribution of the intensity first layer of the protein will result in a uniform binding of the second analyte.

pin to the substrate.

By contrast, in inkjet printing (McWilliam et al., 2011) only the droplets of analyte solution get in contact with the target surface, after being ejected from a nozzle (Barbulovic-Nad et al., 2006). In piezoelectric inkjet printing, a change in voltage alters the pressure in the liquid reservoir and results in droplet formation (Romanov et al., 2014). The advantages of inkjet printing are the very precise calibration of the volume of the droplets, lack of contact between the dispenser and the target surface (Romanov et al., 2014), and the independence of the delivery from surface properties; and its disadvantages, compared with those of pin printing, are the higher technological complexity and lower precision in spot positioning and shape.

Microcontact printing (μCP) makes use of a polydimethylsiloxane (PDMS) stamp to print several spots in parallel directly to the surface (Bernard et al., 1998), and therefore is different from the pin (or contact) and inkjet printing in that it is not a serial, but a parallel technique. The process of μCP involves first the creation of a stamp with the desired pattern on which the protein solution is then adsorbed. Transfer of the solution from the patterned stamp surface to the substrate surface is performed via conformal physical contact and does not require the use of viscous protein solutions (Michel et al., 2001), but is constrained to transferring from a low to a high energy surface, unless humidified microcontact printing is used (Ricoult, 2014). Additionally, μCP, which is capable of printing high resolution, high contrast protein patterns (Filipponi et al., 2016), has the advantage of a soft contact between the carrier, i.e., the stamp, and the target surface. μCP has however the disadvantage of difficult washing of the PDMS stamps, and thus the difficulty of printing high density arrays.

Given the extensive use of pin and inkjet printing in microarray fabrication, as well as the promise of μCP, but also the large differences between the parameters specific to each of these deposition methods, a comprehensive mapping of the quality of protein microarray patterns produced by these techniques is fully justified, and perhaps overdue.

3.2. Input parameters modulating the patterns of protein microarrays

Aside of the physico-chemical processes specific to the used printing technology, the input parameters that also modulate the spot size, morphology and uniformity have three sources: (i) the deposited protein, (ii) the carrier fluid; and (iii) the surface on which the protein is deposited (Bergeron et al., 2015; Ivanova et al., 2006; Moran-Mirabal et al., 2007; Mujawar et al., 2014, 2013, 2012). These three classes of input parameters have been analyzed as follows.

3.2.1. Protein parameters

3.2.1.1. Molecular shape and molecular weight. It was observed (Mujawar et al., 2012) that IgG, with a longer, Y-shaped molecule, produces more uniform spots than BSA, which has a more spherical molecular shape (Supplementary Information, Figure SI1). This is somehow counterintuitive, as layers comprising spherical objects are expected to be more compact (Yunker et al., 2011), thus more uniform. However, the molecular shape relevant to the interaction between the protein and the adsorption surface is the result of the envelope of the molecule by an object with very large radius, i.e., infinite for a geometrically-perfect flat surface, rather than the molecular shape derived from atom-level resolution mapping (Nicolau et al., 2013). Also, both the molecular surface and the molecular surface-to-volume ratio are in a near-univoque relationship with the molecular weight of the protein (Nicolau et al., 2013), which are 150–170 kDa, and 66 kDa, for IgG and BSA, respectively. This results in an actual surface-to-volume ratio, for a near-flat surface (average roughness of 2 nm), of approximately $2\ 10^{-3}\ nm^{-1}$ for IgG and approximately $5\ 10^{-3}\ nm^{-1}$ for BSA (Nicolau et al., 2013). Consequently, and relative to their overall molecular weight, IgG appears to be more compact than BSA, but the flexibility of the molecular conformation, in particular when the protein is in contact with an adsorbing surface, could have an overriding influence.

3.2.1.2. Hydrophobicity and distribution of charges. Other, perhaps more important protein molecular parameters than the molecular surface, weight, and shape, impact on the final structure of the protein layers on surfaces, such as hydrophobicity and distribution of charges. It was found (Nicolau et al., 2014) that only the hydrophobicity manifested on the protein molecular surface is relevant to protein immobilization on surfaces, with the rest of, inner, bulk hydrophobicity having no statistical relevance. The hydrophobicity manifested on the protein molecular surface, both in terms of area and absolute value, is considerably higher for IgG than it is for BSA. Indeed, the hydrophobic areas are approximately 200, and $2\ Å^2$, for IgG and BSA, respectively; and the ratio of hydrophobic/total area are approximately 0.2 and 0.02 for IgG and BSA, respectively (Nicolau et al., 2014). In contrast with hydrophobicity, which is involved in strong, but short

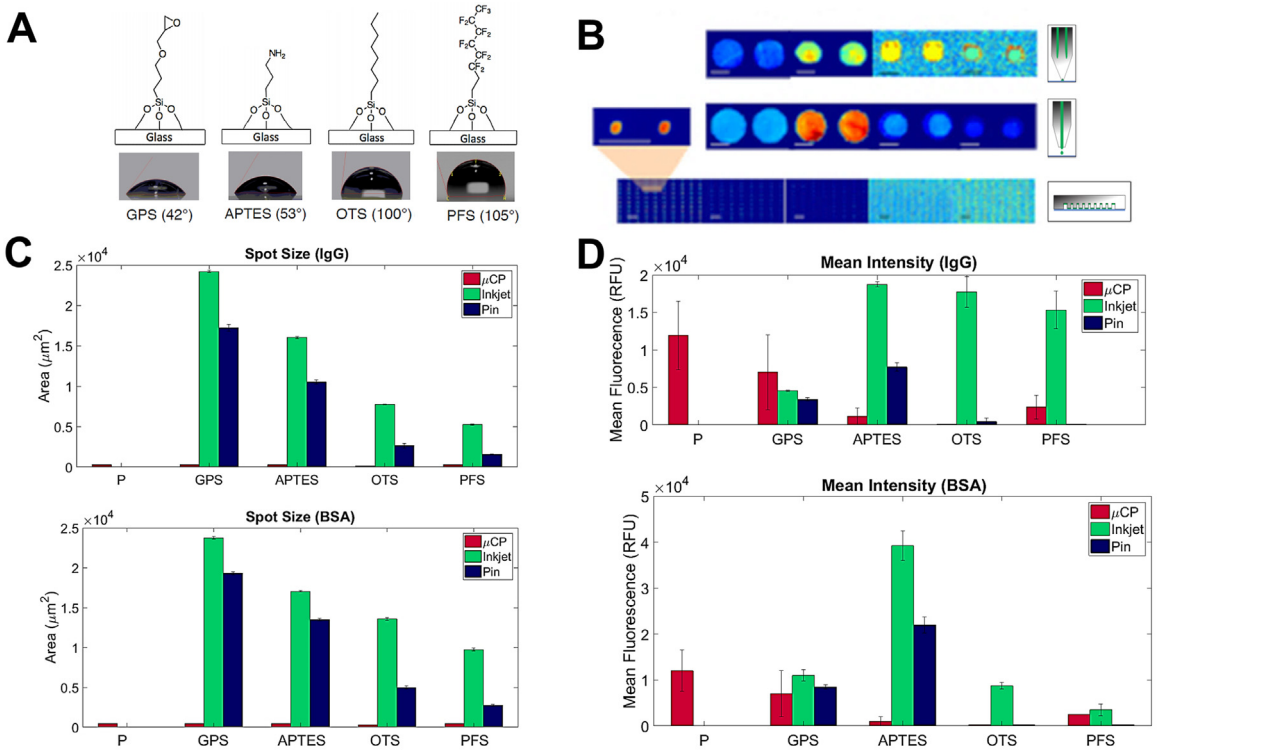

Fig. 2. Printing of proteins on different surfaces of varying chemistries by pin and inkjet printing, and by μCP. A. Schematic illustrating the molecular structure of silane-functionalized glass surfaces, together with their respective contact angles. The contact angle of plasma-treated glass surface is very close to zero. B. Representative images of pin (top), inkjet (middle) and μCP (bottom) printing of 25 μg/ml of BSA on each surface. Scale bars are 100 μm. C. Spot size resulting from μCP, inkjet, and pin printing on plasma-treated glass (P), or GPS-, APTES-, OTS- and PFS-functionalized glass of increasing hydrophobicity (from left to right). D. Mean fluorescence of IgG and BSA spots (25 μg/ml) printed on plasma treated glass (P), GPS-, APTES-, OTS-, and PFS-functionalized glass slides by μCP, inkjet, and pin printing. Note: neither inkjet- nor pin-printing was performed on simply plasma-treated glass slides.

range interactions with the surface, charges will operate through electrostatic interactions, which are weaker, but long range. Consequently, the overall, bulk charges (modulated by the pH of the carrier fluid), rather than those on the molecular surface, will be more relevant to protein immobilization. In that regard, IgG and BSA are again very different, with their isoelectric points at 7.3 ± 1.2, and 4.65, respectively.

To conclude, IgG and BSA are both largely used in protein arrays, for very different functions, but they are also very different in molecular properties, thus constituting valuable case studies.

3.2.2. Parameters of the carrier fluid

To investigate the importance of buffer conditions, IgG and BSA in either PBS or PBSbb have been deposited on organosilane-functionalized surfaces. For inkjet printing, there was no noteworthy difference in the size, or eccentricity of the spots between the two different buffers (Supplementary information Figure SI 4A-B). A more detailed study for the pin printing, also involving the impact of the protein concentration, led to the same conclusion (Supplementary information Figures SI 5 A-D, and SI 6 A-D). However, large increases in the average fluorescence intensity, and a decrease in the 'coffee-ring' ratio (reflecting an increase in uniformity of fluorescence across a spot) were observed for the PBSbb buffer compared with PBS. This provides evidence that hygroscopic additives present in PBSbb increase protein adsorption and decrease the variation of protein density within the spot, which is consistent with previous reports (Bergeron et al., 2015; Dufva, 2005). Moreover, the increase in the fluid viscosity has two follow-up effects. First, a higher viscosity delays the drying process, thereby increasing reaction time with the surface. Second, a higher viscosity will result in a lower diffusivity of the proteins, and therefore will delay their movement towards the edge of the spot. The overlaps of these phenomena result in an increased protein adsorption to the surface and uniformity of deposition.

The impact of the pH of the carrier fluid has possibly important impact on protein adsorption (Nicolau et al., 2014; Ostuni et al., 2001). For instance, the neutral pH of the buffers used in this study is close to the pI of the IgG (7.3) resulting in a near perfect balance between the positive and negative charges of the protein. For BSA however, with a pI at 4.65, the neutral pH will result in a net negative charge of the protein. Consequently, electrostatic interactions will have a smaller impact on the adsorption of a protein with charges in equilibrium, e.g., IgG, which will present a more pronounced propensity for adsorption on hydrophobic surfaces. Conversely, these interactions will play a stronger role for the adsorption of charged proteins, e.g., BSA, in particular if the adsorbing surface present complementary charging.

The optimization of the wash buffer was also performed. For all surfaces tested, the use of the PBST wash buffer decreased the eccentricity and variability of signal intensity within the spot by both droplet-based techniques when compared to washing the slide with simply PBS (Supplementary information SI 7–10). Consequently, in all further analysis comparing inkjet and pin printing, the results are from protein solutions in PBSbb washed with PBST.

3.2.3. Surface parameters

While an increased hydrophobicity of the surface increases the protein adsorption (Ostuni et al., 2003), it also contributes to protein denaturation, via strong hydrophobic interactions with the hydrophobic 'core' of the adsorbed proteins (Hanson et al., 2017; Nicolau et al., 2014). Conversely, hydrophilic surfaces preserve better the protein conformation on the expense of decreased overall protein adsorption (Ostuni et al., 2001).

Self-assembled monolayers (SAMs) are commonly used to change

the physical and chemical properties of a surface by the modification of the chemical groups on the surface. Organosilanes are a widely used for glass or silicon following plasma activation surfaces, since they can form monolayers on multiple surfaces with free hydroxyl groups (Awsiuk et al., 2013; Glass et al., 2011). They are composed of a surface reactive group at one end that chemically binds to the hydroxylated surfaces, a hydrocarbon chain of varying length, and then terminate with a functional group at the other end (Fig. 2A). The terminating functional group is chosen based on the desired application of the surface, e.g., it can promote biomolecular immobilization on the surface, either by physical adsorption, and/or covalent binding, or conversely, it can minimize biomolecule interaction, e.g., a non-fouling surface (Chiu et al., 2010; Kannan et al., 2006).

3.3. Output parameters of the protein pattern

3.3.1. Spot size

To enable the fully automated analysis and quantification of microarray images, the geometrical aspects of the spots should follow an expected shape and be highly reproducible in size (Draghici et al., 2003). Beyond just data processing, the reproducibility of the primary protein spot size ensures that there is an equal spot surface area accessible to secondary biomolecules for binding, with further beneficial impact on the reliability of detection.

Both droplet-based techniques produced spots with distinctly different characteristics. First, as expected, the spot sizes resulting from pin and inkjet printing were considerably larger than those obtained by μCP (Fig. 2B,C). Second, the spot size resulting from both droplet-based techniques was in an inverse relationship with the contact angle of the surface, whereas for μCP, the spot size does not depend on surface hydrophobicity (Fig. 2C). This general trend with droplet-based techniques agrees with previous investigations into the relationship between the size of a droplet and the target surface (Mujawar et al., 2013; Vafaei and Podowski, 2005). The size of the spot produced by μCP is determined by the conformal contact of the calibrated stamp to the surface, whereas for the droplet-based techniques the spot size is dependent on the shape of the droplet on the surface, which, in turn, is dependent of the surface tension of the adsorbing surface.

Due to the large differences in sizes of the spots produced by droplet techniques, on one side, and μCP on the other, the analysis will treat these cases separately.

In the present study, the automatic segmentation of the spots from the background was aided by *a priori* information on the expected spot size. The printing that produced a consistent spot size meant that any fluorescent artifacts on the slide outside of the expected size range could be automatically removed from analysis. Therefore, the automatic spot segmentation and analysis is aided when there is a limited expected size range of the printed spots. To quantify the regularity of spot size, the relative standard deviation of the spot size was calculated by dividing the standard deviation from each triplicate measurement by its mean spot size, i.e., relative standard deviation = (standard deviation)/mean.

Spot size regularity, i.e., the ratio between the standard deviation of the spot size by its mean (Supplementary information, Glossary), is dependent on the surface hydrophobicity and the protein concentration (Supplementary Figure SI 11). In general, the size variability increases as the surface hydrophobicity increases, which can be statistically attributed to a decrease in spot size, and subsequent quantification errors. Using this metric, the inkjet printing presents a lower variation in the relative standard deviation compared to pin printing (with the exception of PFS surfaces). These observations can be explained by the use of more than one pin in pin printing, as compared to the single nozzle used in inkjet printing (Supplementary Figure SI 5, SI 6, and SI 12).

3.3.2. Signal intensity

The quantification of the protein surface concentration on each surface was performed by measuring the intensity of the fluorescence signal of the two different fluorescent-labelled proteins. As expected, for each protein, the surface, and method used, the mean fluorescent intensity decreased with the decrease of the concentration of protein in solution (Fig. 2D, and Supplementary information, Figs. S1 13). For both droplet-based techniques, the spots presented the highest mean intensity of BSA and IgG on APTES slides than on any other substrate (Fig. 2D). This observation supports the evidence that using APTES is an efficient surface modification method to promote protein immobilization (Anand et al., 2010; Awsiuk et al., 2012, 2013).

The fluorescence signal of IgG and BSA patterns on the *hydrophilic* GPS-functionalized surfaces using the droplet-based techniques was particularly low (Fig. 2D). Because previous works have found that proteins can form covalent bonds with the GPS epoxide group, the low level of immobilization on GPS surfaces could be a result of the slow reaction kinetics at neutral pH (Awsiuk et al., 2012) and short incubation time (two hours).

Interestingly, the adsorption of both IgG and BSA on the *hydrophobic* OTS and PFS surfaces is lower than on the hydrophilic APTES surface, likely due to the differences in their surface chemistry. The hydrophobic OTS substrate is composed of a long hydrocarbon chain that will minimally bind with the hydrophilic molecular surface of proteins (Russo et al., 2011). Additionally, the binding with the bulky hydrocarbon chain of OTS lowers the entropy of proteins remaining in solution by means of steric hindrance (Russo et al., 2011). Also, PFS is commonly used to create water and oil-repellent surfaces and to prevent PDMS from irreversibly adhering to another layer of PDMS when replicating a PDMS pattern (Glass et al., 2011; Pujari et al., 2014). Previous studies have shown that these surface modifications prevent the non-specific adsorption of proteins, e.g., BSA, streptavidin, R-phycoerythrin, to the surface (Kim et al., 2011; Kira et al., 2009; Takashi et al., 2005). These observations offer explanations for the low immobilization levels for BSA and IgG on both OTS and PFS surface.

In contrast with the droplet-based techniques, the spots produced by μCP showed a decrease in mean intensity as the contact angle of the surface increased (Fig. 2D). This confirms that μCP in dry conditions has the greatest transfer efficiency from a low-energy (hydrophobic) PDMS stamp to a high-energy (hydrophilic) substrate (Romanov et al., 2014).

3.3.3. Spot morphology

For the majority of microarray investigations, the analysis of the spot quality is qualitatively determined based on the spot circularity and/or by calculating the percent standard deviation of the fluorescence signal, i.e., the standard deviation of fluorescence within the spot divided by the mean fluorescence (Bergeron et al., 2015; Bietsch et al., 2004; Moran-Mirabal et al., 2007; Mujawar et al., 2013). However, the limitations of these metrics include the possible human bias, and that the percent standard deviation does not provide any information on the type of spot inhomogeneity. Consequently, a more comprehensive analysis is warranted.

The uneven deposition of protein solutions during the drying process can result in “coffee-ring” spots, i.e., higher deposition at the contact line; or ‘bull's eye’ spots, i.e., higher deposition of solutes in the center of the spot (Fig. 3). The evaporation of a droplet on a solid surface is governed by gravity, hydrodynamic flow, Marangoni flow (if a temperature or concentration gradient arises during drying), and the pinning at the liquid-air interface, i.e., the contact line (Erbil, 2012). The ‘coffee-ring’ spots result when the evaporating droplet has a pinned contact line, high evaporation rate at the surface of the droplet, and/or when there is a suppressed Marangoni flow (Hu and Larson, 2006). Conversely, rapid evaporation and the absence of a pinned contact line results in increased deposition in the middle of the spot (a ‘bull's eye’ feature).

The eccentricity, defined as the ratio of the distance between the center of a spot and its major axis length (Supplementary information, Glossary), quantifies the deviation of a spot shape from a perfect circle.

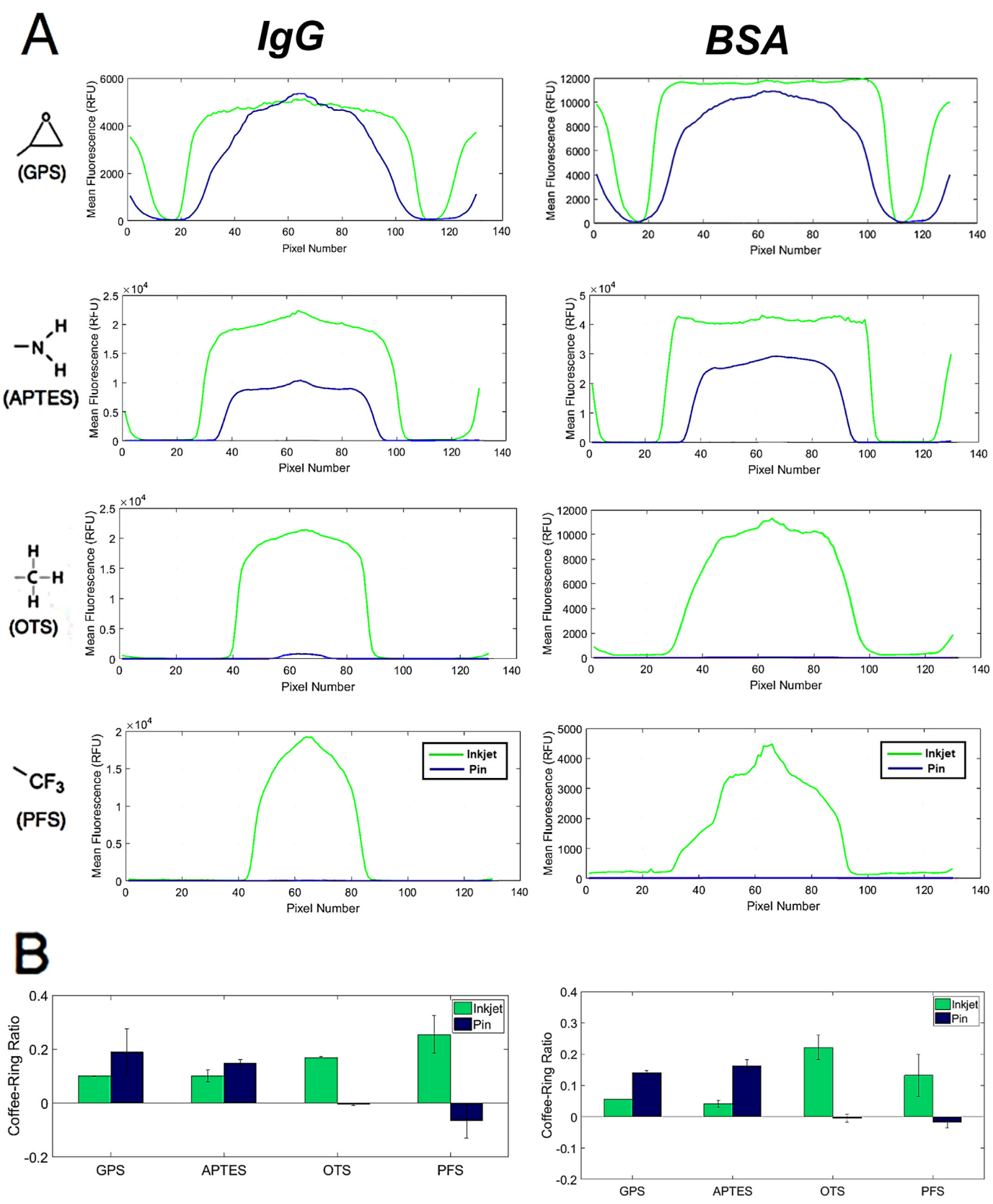

Fig. 3. Fluorescence signal intensity profiles and corresponding 'coffee-ring' ratios of printed protein spots. A. Profiles representing the intensity profile across protein spots of 25 μg/ml of IgG and BSA printed on silane-functionalized glass by inkjet (blue) and pin printing (green). B. CRR values of IgG and BSA (25 μg/ml) spots printed on silane-functionalized glass by inkjet (blue) and pin printing (green). Error bars represent the standard errors. (For interpretation of the references to color in this figure legend, the reader is referred to the web version of this article).

An eccentricity value of zero represents a perfect circle with a constant radius around the central axis, and a value of one represents a line.

A significant increase in the eccentricity of the spots has been observed, for both droplet-based methods, for those printed on hydrophobic surfaces (OTS and PFS), as opposed to those printed on hydrophilic ones (GPS and APTES). Inkjet printing on the GPS surface produced spots with significantly lower eccentricity than on any other surface. In addition, spot eccentricity increased with surface hydrophobicity. For pin printing, there was no significant difference in the eccentricity between hydrophilic surfaces, although eccentricity did significantly increase on hydrophobic surfaces. Between the two droplet-based techniques, pin printing produced significantly more eccentric circles than inkjet printing on all substrates, except PFS (Fig. 3). The fact that pin printing produces less circular spots, may be the result of the square footprint of the silicon pin touching the surface while depositing a droplet. The eccentricity measure for both methods did not significantly differ across protein concentration (Supplementary information Figure SI 6).

3.3.4. Spot uniformity

The uniformity of the fluorescence within a spot was dependent, in a complex manner, on the droplet-based printing method, surface properties (as presented in Fig. 3), and the concentration of the protein in solution (Fig. 4 for OTS surfaces, and Supplementary information Figures SI 7–10, in the context of analysing the effect of the washing conditions).

For both droplet-based methods, the delineation of the spot edge, i.e., image contrast, was the highest on the APTES surface, followed by the GPS one. As the hydrophobicity of the surface increases, the receding of the inkjet droplet from the initial contact line to the center is apparent by a shallow slope of the signal intensity that creates a less defined spot edge. In addition to the surface properties impacting the delineation of the spot edge, the contrast of the spot was clearer for the inkjet than for pin printing due to a steeper slope of the intensity profile. The inkjet printing of BSA on hydrophobic surfaces (OTS and PFS) exhibited a quasi-step-wise fluorescent pattern (Fig. 4 and Supplementary Figure SI 9–10). It was argued (Askounis et al., 2015) that this drying morphology is due to a 'stick-slip' mechanism that, like in the 'coffee-ring' pattern, is the result of pinning at the liquid-air interface. However, the process differs from the 'coffee-ring' morphology since the contact line is pinned at one side only. As evaporation occurs, a critical contact angle is reached and the droplet recedes to a new liquid-air interface line towards the immobilized contact line. This process results in a pattern comprising concentric rings, or the 'half-moon' morphology. Also the pattern is more pronounced on hydrophobic surfaces that have a higher critical contact angle (Askounis et al., 2015).

The plateau of the fluorescent intensity profile, or its minimal curvature, was again dependent on the droplet printing method, the surface properties, and the concentration of the protein in solution. The pin printing produced spots with the smoothest profile on APTES, while inkjet printing produced the smoothest profile on the GPS surface. Interestingly, the profiles of the BSA spots were smoother than those for IgG on the hydrophilic surfaces, whereas the opposite was observed on hydrophobic surfaces.

On hydrophilic surfaces, i.e., APTES and GPS, a positive 'coffee-ring' ratio, CRR, indicating a 'bull's eye' spot morphology, was regularly produced by both droplet-based methods (Fig. 3). Based on the CRR, the inkjet printing produced more uniform spots on hydrophilic surfaces than those produced by pin printing. Conversely, on hydrophobic surfaces, i.e., OTS and PFS, the spot morphology was dependent on the method used (Figs. 3 and 4). Inkjet printing produced a positive CRR of higher value, pointing to an even more pronounced 'bull's eye' morphology than that observed on hydrophilic surfaces. The pin printing patterns are characterised by a negative CRR when dilute protein solutions were printed on hydrophobic surfaces, exhibiting a 'coffee-ring' spot morphology. The strength of the CRR as a metric to measure differences in the type of spot homogeneity is evident by the fact that it can delineate between, and quantifies of the differences in signal irregularities that would be difficult to decipher by the human eye alone.

The fact that pin printing creates a negative 'coffee-ring' ratio on hydrophobic surfaces could be the result of the transfer of proteins from the edge of the pin. In pin printing, the pin touches the substrate, then transfers the droplet on the surface. The volume of this droplet is governed by the contact angle of the substrate. On a substrate with a higher contact angle, the resulting droplet has a smaller contact area with the surface than the area that the pin head originally contacted. At high protein solution concentrations this results in a very small spot of high intensity within the printed spot. This spot morphology would normally be considered 'bull's eye'-like, however, it has a zero, or negative 'coffee-ring' ratio because the number of pixels in this very small spot within the overall spot are not large enough to offset all the pixels in the outer 50% of the spot. A separate spot morphology at lower protein concentrations on OTS and PFS presents a concentric circle or 'half-moon' pattern that explains the resulting negative 'coffee-ring' ratio.

The relative standard deviation (RSD) of the signal intensity is another metric used to quantify its uniformity (Diehl et al., 2001). Based on the RSD, the PFS surface induced the highest signal non-uniformity for printing of both proteins, by both droplet-based methods, and for all

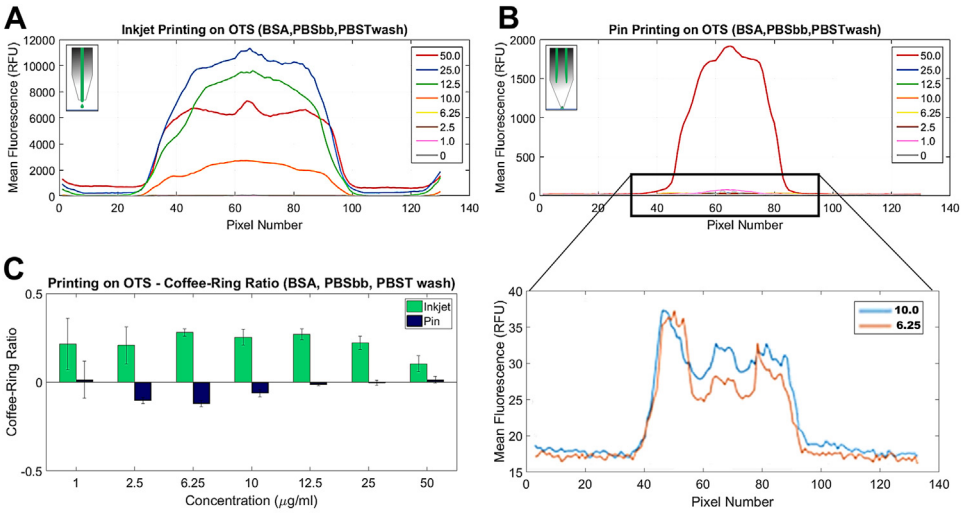

Fig. 4. Fluorescent intensity profiles of spots printed with inkjet (A) and pin (B) printing on an OTS-functionalized surface for various BSA concentrations. C. 'Coffee-ring' ratio of 1.0 μg/ml to 50 μg/ml BSA solution printed on OTS-functionalized surface by inkjet and pin printing. D. Detail of intensity profile for low concentrations of BSA for pin printing.

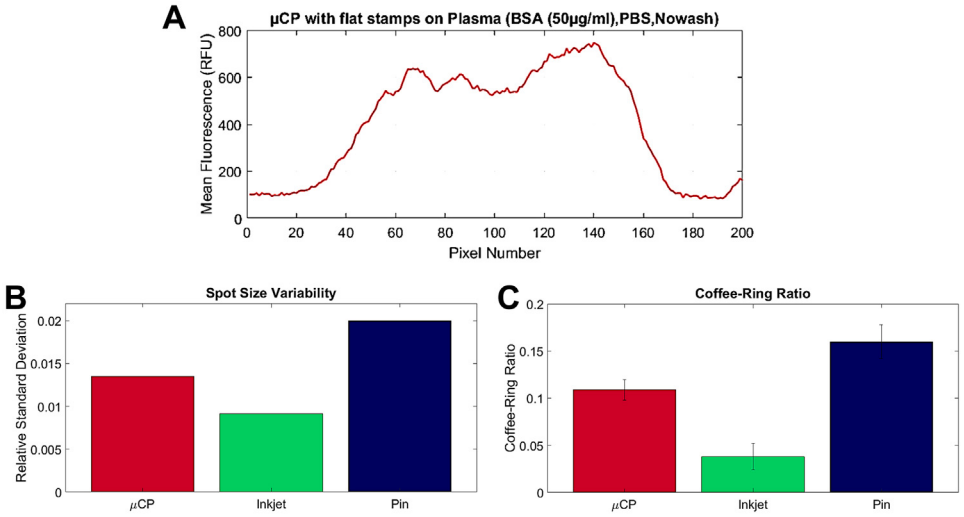

Fig. 5. Uniformity analysis of protein spots printed by μCP compared to the droplet-based techniques. A. Fluorescent intensity profile of BSA spots (50 μg/ml) printed on a plasma-treated glass using μCP, from high resolution image. Spot size variability (B) and 'coffee-ring' ratio (C) of BSA (50 μg/ml) spots printed by μCP on plasma-treated glass surface; and of BSA (25 μg/ml) of inkjet and pin printed on APTES-functionalized slides.

concentrations of proteins in solution. The RSD, like the CRR, was dependent on the protein concentration. Instances where the RSD was high were due to the large signal intensity differences between replicate trials, i.e., slide-to-slide variations. The calculation of RSD within each slide would provide further information on intra-slide variations, but still would not provide any information regarding the inhomogeneity within a spot.

3.3.5. *Spot analysis for micro-contact printing*

The μCP technique was analyzed separately because the resulting spots were approximately a hundred times smaller than those resulting from the droplet-based techniques. The results (Fig. 5) show that a relatively uniform protein layer is produced, with a high contrast between the signal and the background. However, the top of the profile is not smooth, suggesting that more protein is transferred at the one edge of the PDMS, possibly due to the uneven pressure applied to the stamp.

The uniformity of the μCP spots was superior on a plasma-treated glass surface when compared to the spots resulting from the droplet-based techniques on the APTES surface (Supplementary information, Figure SI 14, for all surfaces; and Figure SI 13). As presented in Fig. 5, the uniformity of the μCP spots, based on spot size variability and the 'coffee-ring' ratio, was comparable to the droplet-based techniques.

3.4. *Overall comparison of spot parameters*

The price for the elegance and simplicity of microarray technology is the high phenomenological complexity of the processes involved in protein patterning on surfaces. Additionally, the technological input variables have very different nature. For instance, the deposition methods and the proteins are 'classes' of experimental variables, whereas the concentration of the proteins in solution can be numerically quantified. Other input variables, e.g., surfaces, can be partially compared using one important, but not exclusive, parameter, e.g., surface hydrophobicity quantified by their contact angle. The complexity of the phenomenological processes and technological input variables involved in microarray fabrication asked, by necessity, a combinatorial experimentation approach. Indeed, in this study, six input technological variables, i.e., deposition methods (3), proteins (2), protein concentrations (7), buffers (2) surfaces (5), and washing solutions (2), have been mapped to assess the performance of various combinations of the microarray technological process. The mapping of these technological variables resulted in more than 800 separate experiments, each with at least five replicates to ensure the statistical relevance of the results. The comprehensive nature of the mapping of the input variables is mirrored by the variety of the technological output variables for microarray fabrication, which quantifies its performance, namely spot size, size variability, eccentricity, mean intensity, coffee ring ratio, contrast, and smoothness. To this end, in order to synthetically assess the modulation of microarray protein spots by input technological parameters, IgG and BSA protein patterns produced by inkjet, pin, and μCP, on silane-functionalized and plasma-treated glass, have been analyzed versus the seven process performance output variables.

For a synthetic comparison, all of the investigated parameters were integrated into a radar chart to visualise their impact on the key performance parameters of microarray protein patterns (Fig. 6). The spot size and eccentricity values used for comparison are based on the printing with a 12.5 μg/ml solution, as these values were the most consistent with regard to these two performance criteria. The results from the 25 μg/ml solution were used to compare the mean intensity values since below this concentration μCP resulted in very low values. Since there was no clear trend for the 'coffee-ring' ratio, or spot size variability with concentration, the value of each of these variables was added across concentrations for each method to produce the resulting value used for comparison. The qualitative measurements of smoothness and contrast observed in the intensity profiles of the 25 μg/ml spots were given a value of 1–4, wherein 1 represented a profile without significant intensity for comparison, and 4 represented the best method on that surface. For variables where a number close to zero reflected a better printing method, i.e., 'coffee-ring' ratio and eccentricity, the quantified value was subtracted from 1, and therefore a higher value represents better performance. The spot size is the one variable where the value was used for direct comparison and does not reflect one method being better than another. All quantitative values were normalized to 1. The results of this comparison are presented in Fig. 6.

Inkjet printing produced spots with a higher contrast between the spot and background signal, on all surfaces, as compared to pin printing, as demonstrated by a steeper slope of their profile of the fluorescence signal. The size of the spots produced by inkjet printing was more uniform than those produced by pin printing. Also, the necessity of having multiple pins to enable higher throughput increases the variability between spots. On hydrophobic surfaces pin printing produced 'coffee-ring' spots, whereas inkjet printing produced 'bull's eye' spots. The smoothness of the fluorescent profile and the cumulative 'coffee-ring' ratio across concentrations were comparable for both pin and inkjet printing demonstrating that the two methods produce spots of similar uniformity during the deposition process.

The use of the hygroscopic additives betaine and 2,3-butanediol increased the circularity, uniformity, and mean fluorescence intensity of the spots printed using a droplet-based method, as previously

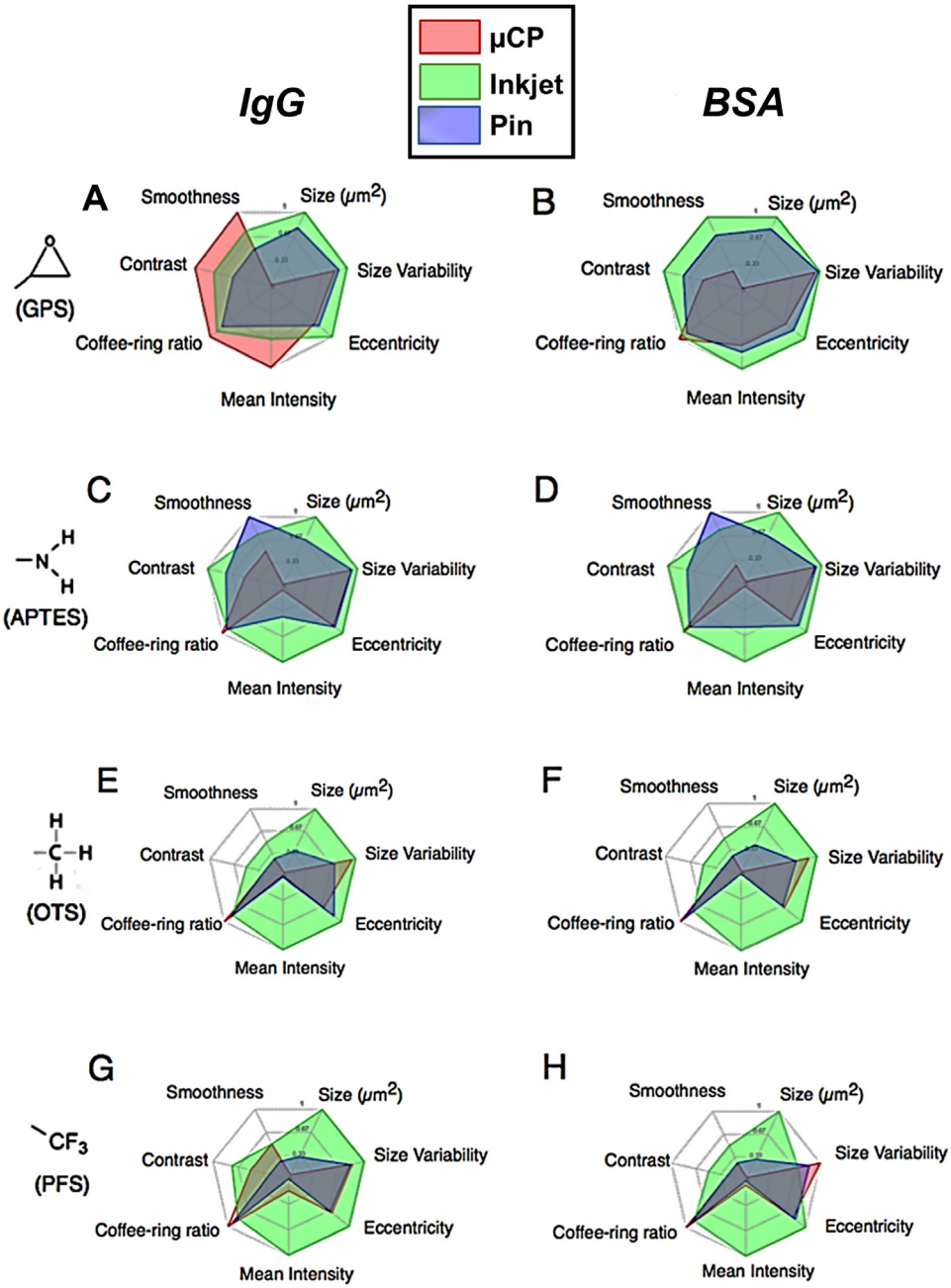

Fig. 6. Performance of deposition techniques. Radar charts show how the three methods, i.e., μCP (red), inkjet (green), and pin (blue) printing, compare against the seven performance criteria investigated in this work, for printing IgG (left), and BSA (right), on GPS- (A, B), APTES- (C, D), OTS- (E, F), and PFS-functionalized (G, H) glass slides. For each parameter, except size, a larger area covered represents a better performance of the method for this parameter. (For interpretation of the references to color in this figure legend, the reader is referred to the web version of this article).

demonstrated (Bergeron et al., 2015). A wash buffer following printing that included the detergent Tween-20 decreased the variability in the size and uniformity of the printed spots when compared to a mild wash buffer without detergent. This highlights the importance of buffer composition and printing parameter optimization to produce high quality protein microarrays.

The comparative analysis of the spots produced by μCP is more difficult, due to the small stamps used, and consequently the fewer pixels per spot. However, when a higher resolution image is considered, a clearer contrast was evident. This demonstrates that μCP can produce much smaller spots with comparable uniformity to inkjet and pin printing. In future work the results of using larger stamps to create spots of comparable size to the droplet-based techniques should be investigated to adequately compare methods.

4. Conclusion

To map the modulation of microarray protein spots by technological parameters, IgG and BSA protein patterns produced by inkjet, pin, and microcontact printing (μCP) on silane-functionalised glass have been analyzed versus spot size, size, eccentricity, mean fluorescence intensity, 'coffee-ring' ratios, and the contrast and smoothness of the fluorescence intensity profile.

The printing on APTES-functionalized glass using droplet-based techniques produced superior quality spots than any other surface. Inkjet printing resulted in a higher quality of the spots on the widest

range of surfaces compared to pin printing, largely because the deposition of the protein solution does not depend on the substrate surface. μCP was also shown to produce quality spots that are much smaller than what either inkjet, or pin printing, are capable. However, the high transfer efficiency of the μCP was limited to hydrophilic, high energy surfaces, consistent with prior results (Ricoult et al., 2014).

Whereas other factors, such as secondary biomolecule binding and microenvironment conditions, could affect the final efficacy of the microarray, the strong correlation between immobilized protein and binding signal suggests that the strongest and most homogeneous signals generally lead to the best performing microarrays. This work introduces a systematic approach for the assessment of the quality of spot microarrays and the results presented can be used as a methodological template for the optimization of the development of future protein microarrays. Depending on the specific microarray application, future work is need to further study, using similar procedures as detailed here, the impact of input parameters on the secondary microarray pattern, so that the best combination of the printing method, surface and carrier fluid can be chosen.

Acknowledgements

The research was supported by a Natural Sciences and Engineering Research Council (NSERC) Discovery Project No 238925, and by a fellowship provided by McGill Institute for Advanced Materials (MIAM).

Appendix A. Supporting information

Supplementary data associated with this article can be found in the online version at doi:10.1016/j.bios.2018.09.027.

References

Anand, G., Sharma, S., Dutta, A.K., Kumar, S.K., Belfort, G., 2010. Conformational transitions of adsorbed proteins on surfaces of varying polarity. Langmuir 26 (13), 10803–10811.
Anderson, K.S., Sibani, S., Wallstrom, G., Qiu, J., Mendoza, E.A., Raphael, J., Hainsworth, E., Montor, W.R., Wong, J., Park, J.G., Lokko, N., Logvinenko, T., Ramachandran, N., Godwin, A.K., Marks, J., Engstrom, P., LaBaer, J., 2011. Protein microarray signature of autoantibody biomarkers for the early detection of breast cancer. J. Proteome Res. 10 (1), 85–96.
Angulo, J., 2008. Polar modelling and segmentation of genomic microarray spots using mathematical morphology. Image Anal. Stereol. 27 (2), 107–124.
Askounis, A., Sefiane, K., Koutsos, V., Shanahan, M.E., 2015. Effect of particle geometry on triple line motion of nano-fluid drops and deposit nano-structuring. Adv. Colloid Interface Sci. 222, 44–57.
Austin, J., Holway, A.H., 2011a. Contact printing of protein microarrays. Methods Mol. Biol. 785, 379–394.
Austin, J., Holway, A.H., 2011b. Contact printing of protein microarrays. Methods Mol. Biol. 379–394.
Avseenko, N.V., Morozova, T.Y., Ataullakhanov, F.I., Morozov, V.N., 2002. Immunoassay with multicomponent protein microarrays fabricated by electrospray deposition. Anal. Chem. 74 (5), 927–933.
Awsiuk, K., Bernasik, A., Kitsara, M., Budkowski, A., Petrou, P., Kakabakos, S., Prauzner-Bechcicki, S., Rysz, J., Raptis, I., 2012. Spectroscopic and microscopic characterization of biosensor surfaces with protein/amino-organosilane/silicon structure. Colloids Surf. B Biointerfaces 90, 159–168.
Awsiuk, K., Budkowski, A., Psarouli, A., Petrou, P., Bernasik, A., Kakabakos, S., Rysz, J., Raptis, I., 2013. Protein adsorption and covalent bonding to silicon nitride surfaces modified with organo-silanes: comparison using AFM, angle-resolved XPS and multivariate ToF-SIMS analysis. Colloids Surf. B Biointerfaces 110, 217–224.
Babel, I., Barderas, R., Díaz-Uriarte, R., Martínez-Torrecuadrada, J.L., Sánchez-Carbayo, M., Casal, J.I., 2009. Identification of tumor-associated autoantigens for the diagnosis of colorectal cancer in serum using high density protein microarrays. Mol. Cell. Proteom. 8 (10), 2382–2395.
Barbulovic-Nad, I., Lucente, M., Sun, Y., Zhang, M., Wheeler, A.R., Bussmann, M., 2006. Bio-microarray fabrication techniques–a review. Crit. Rev. Biotechnol. 26 (4), 237–259.
Bergeron, S., Laforte, V., Lo, P.S., Li, H., Juncker, D., 2015. Evaluating mixtures of 14 hygroscopic additives to improve antibody microarray performance. Anal. Bioanal. Chem. 407 (28), 8451–8462.
Bernard, A., Delamarche, E., Schmid, H., Michel, B., Bosshard, H.R., Biebuyck, H., 1998. Printing patterns of proteins. Langmuir 14 (9), 2225–2229.
Bietsch, A., Hegner, M., Lang, H.P., Gerber, C., 2004. Inkjet deposition of alkanethiolate monolayers and DNA oligonucleotides on gold: evaluation of spot uniformity by wet etching. Langmuir 20 (12), 5119–5122.
Chiu, C.S., Lee, H.M., Gwo, S., 2010. Site-selective biofunctionalization of aluminum nitride surfaces using patterned organosilane self-assembled monolayers. Langmuir 26 (4), 2969–2974.
Cui, L., Zhang, J., Zhang, X., Huang, L., Wang, Z., Li, Y., Gao, H., Zhu, S., Wang, T., Yang, B., 2012. Suppression of the coffee ring effect by hydrosoluble polymer additives. ACS Appl. Mater. Interfaces 4 (5), 2775–2780.
Deforest, C.A., Tirrell, D.A., 2015. A photoreversible protein-patterning approach for guiding stem cell fate in three-dimensional gels. Nat. Mater. 14 (5), 523–531.
Diehl, F., Grahlmann, S., Beier, M., Hoheisel, J.D., 2001. Manufacturing DNA microarrays of high spot homogeneity and reduced background signal. Nucleic Acids Res. 29 (7).
Draghici, S., Lenhart, S., Safer, H., Maini, P., Etheridge, A., Gross, L., 2003. Data Analysis Tools for DNA Microarrays. Chapman and Hall/CRC, New York.
Dufva, M., 2005. Fabrication of high quality microarrays. Biomol. Eng. 22 (5–6), 173–184.
Erbil, H.Y., 2012. Evaporation of pure liquid sessile and spherical suspended drops: a review. Adv. Colloid Interface Sci. 170 (1–2), 67–86.
Filipponi, L., Livingston, P., Kašpar, O., Tokárová, V., Nicolau, D.V., 2016. Protein patterning by microcontact printing using pyramidal PDMS stamps. Biomed. Micro. 18 (1), 1–7.
Glass, N.R., Tjeung, R., Chan, P., Yeo, L.Y., Friend, J.R., 2011. Organosilane deposition for microfluidic applications. Biomicrofluidics 5 (3), 36501–365017.
Hanson, K.L., Fulga, F., Dobroiu, S., Solana, G., Kaspar, O., Tokarova, V., Nicolau, D.V., 2017. Polymer surface properties control the function of heavy meromyosin in dynamic nanodevices. Biosens. Bioelectron. 93, 305–314.
Harwanegg, C., Hiller, R., 2005. Protein microarrays for the diagnosis of allergic diseases: state-of-the-art and future development. Clin. Chem. Lab. Med. CCLM/FESCC 43 (12), 1321–1326.
Hu, H., Larson, R.G., 2006. Marangoni effect reverses coffee-ring depositions. J. Phys. Chem. B 110 (14), 7090–7094.
Ivanova, E.P., Wright, J.P., Pham, D., Filipponi, L., Viezzoli, A., Nicolau, D.V., 2002. Polymer microstructures fabricated via laser ablation used for multianalyte protein microassay. Langmuir 18 (24), 9539–9546.
Ivanova, E.P., Wright, J.P., Pham, D.K., Brack, N., Pigram, P., Alekseeva, Y.V., Demyashev, G.M., Nicolau, D.V., 2006. A comparative study between the adsorption and covalent binding of human immunoglobulin and lysozyme on surface-modified poly(tert-butyl methacrylate). Biomed. Mater. 1 (1), 24–32.
Kannan, B., Castelino, K., Chen, F.F., Majumdar, A., 2006. Lithographic techniques and surface chemistries for the fabrication of PEG-passivated protein microarrays. Biosens. Bioelectron. 21 (10), 1960–1967.
Kim, D.J., Lee, J.M., Park, J.G., Chung, B.G., 2011. A self-assembled monolayer-based micropatterned array for controlling cell adhesion and protein adsorption. Biotechnol. Bioeng. 108 (5), 1194–1202.
Kira, A., Okano, K., Hosokawa, Y., Naito, A., Fuwa, K., Yuyama, J., Masuhara, H., 2009. Micropatterning of perfluoroalkyl self-assembled monolayers for arraying proteins and cells on chips. Appl. Surf. Sci. 255 (17), 7647–7651.
Kumble, K.D., 2007. An update on using protein microarrays in drug discovery. Expert Opin. Drug Discov. 2 (11), 1467–1476.
Laforte, V., Olanrewaju, A., Juncker, D., 2013. Low-cost, high liquid volume silicon quill pins for robust and reproducible printing of antibody microarrays. In: Proceedings of the 17th International Conference on Miniaturized Systems for Chemistry and Life Sciences, MicroTAS, pp. 485–487.
Launiere, C., Gaskill, M., Czaplewski, G., Myung, J.H., Hong, S., Eddington, D.T., 2012. Channel surface patterning of alternating biomimetic protein combinations for enhanced microfluidic tumor cell isolation. Anal. Chem. 84 (9), 4022–4028.
Lee, H.J., Wark, A.W., Corn, R.M., 2008. Microarray methods for protein biomarker detection. Analyst 133 (8), 975–983.
Lee, K.B., Kim, E.Y., Mirkin, C.A., Wolinsky, S.M., 2004. The use of nanoarrays for highly sensitive and selective detection of human immunodeficiency virus type 1 in plasma. Nano Lett. 4 (10), 1869–1872.
McWilliam, I., Kwan, M.C., Hall, D., 2011. Inkjet printing for the production of protein microarrays. Methods Mol. Biol. 345–361.
Michel, B., Bernard, A., Bietsch, A., Delamarche, E., Geissler, M., Juncker, D., Kind, H., Renault, J.P., Rothuizen, H., Schmid, H., Schmidt-Winkel, P., Stutz, R., Wolf, H., 2001. Printing meets lithography: soft approaches to high-resolution patterning. IBM J. Res. Dev. 45 (5), 697–719.
Moran-Mirabal, J.M., Tan, C.P., Orth, R.N., Williams, E.O., Craighead, H.G., Lin, D.M., 2007. Controlling microarray spot morphology with polymer liftoff arrays. Anal. Chem. 79 (3), 1109–1114.
Mujawar, L.H., Kuerten, J.G.M., Siregar, D.P., van Amerongen, A., Norde, W., 2014. Influence of the relative humidity on the morphology of inkjet printed spots of IgG on a non-porous substrate. RSC Adv. 4 (37), 19380–19388.
Mujawar, L.H., Norde, W., van Amerongen, A., 2013. Spot morphology of non-contact printed protein molecules on non-porous substrates with a range of hydrophobicities. Analyst 138 (2), 518–524.
Mujawar, L.H., van Amerongen, A., Norde, W., 2012. Influence of buffer composition on the distribution of inkjet printed protein molecules and the resulting spot morphology. Talanta 98, 1–6.
Müller, U.R., Nicolau, D.V. (Eds.), 2005. Microarray Technology and Its Applications. Springer Berlin Heidelberg.
Nicolau, D.V., Ivanova, E.P., Fulga, F., Filipponi, L., Viezzoli, A., Dobroiu, S., Alekseeva, Y.V., Pham, D.K., 2010. Protein immobilisation on micro/nanostructures fabricated by laser microablation. Biosens. Bioelectron. 26 (4), 1337–1345.
Nicolau, D.V., Paszek, E., Fulga, F., Nicolau, D.V., 2014. Mapping hydrophobicity on the protein molecular surface at atom-level resolution. PLoS One 9 (12).

Nicolau, D.V., Paszek, E., Fulga, F., Nicolau Jr, D.V., 2013. Protein molecular surface mapped at different geometrical resolutions. PLoS One 8 (3).
Nicolau, D.V., Suzuki, H., Mashiko, S., Taguchi, T., Yoshikawa, S., 1999a. Actin motion on microlithographically functionalized myosin surfaces and tracks. Biophys. J. 77 (2), 1126–1134.
Nicolau, D.V., Taguchi, T., Taniguchi, H., Tanigawa, H., Yoshikawa, S., 1999b. Patterning neuronal and glia cells on light-assisted functionalised photoresists. Biosens. Bioelectron. 14 (3), 317–325.
Ostuni, E., Chapman, R.G., Holmlin, R.E., Takayama, S., Whitesides, G.M., 2001. A survey of structure-property relationships of surfaces that resist the adsorption of protein. Langmuir 17 (18), 5605–5620.
Ostuni, E., Grzybowski, B.A., Mrksich, M., Roberts, C.S., Whitesides, G.M., 2003. Adsorption of proteins to hydrophobic sites on mixed self-assembled monolayers. Langmuir 19 (5), 1861–1872.
Pujari, S.P., Scheres, L., Marcelis, A.T., Zuilhof, H., 2014. Covalent surface modification of oxide surfaces. Angew. Chem. Int. Ed. Engl. 53 (25), 6322–6356.
Qu, H., Wang, H., Huang, Y., Zhong, W., Lu, H., Kong, J., Yang, P., Liu, B., 2004. Stable microstructured network for protein patterning on a plastic microfluidic channel: strategy and characterization of on-chip enzyme microreactors. Anal. Chem. 76 (21), 6426–6433.
Renault, J.P., Bernard, A., Juncker, D., Michel, B., Bosshard, H.R., Delamarche, E., 2002. Fabricating microarrays of functional proteins using affinity contact printing. Angew. Chem. Int. Ed. 41 (13), 2320–2323.
Ricoult, S.G., Nezhad, A.S., Knapp-Mohammady, M., Kennedy, T.E., Juncker, D., 2014. Humidified microcontact printing of proteins: universal patterning of proteins on both low and high energy surfaces. Langmuir 30 (40), 12002–12010.
Romanov, V., Davidoff, S.N., Miles, A.R., Grainger, D.W., Gale, B.K., Brooks, B.D., 2014. A critical comparison of protein microarray fabrication technologies. Analyst 139 (6), 1303–1326.
Russo, P.A., Ribeiro Carrott, M.M.L., Mourão, P.A.M., Carrott, P.J.M., 2011. Tailoring the surface chemistry of mesocellular foams for protein adsorption. Colloids Surf. A: Physicochem. Eng. Asp. 386 (1), 25–35.
Saeed, A.I., Sharov, V., White, J., Li, J., Liang, W., Bhagabati, N., Braisted, J., Klapa, M., Currier, T., Thiagarajan, M., Sturn, A., Snuffin, M., Rezantsev, A., Popov, D., Ryltsov, A., Kostukovich, E., Borisovsky, I., Liu, Z., Vinsavich, A., Trush, V., Quackenbush, J., 2003. TM4: a free, open-source system for microarray data management and analysis. Biotechniques 34 (2), 374–378.
Schena, M., Shalon, D., Davis, R.W., Brown, P.O., 1995. Quantitative monitoring of gene expression patterns with a complementary DNA microarray. Science 270 (5235), 467–470.
Štulík, J., 2011. In: Štulík, J. (Ed.), BSL3 and BSL4 Agents: Proteomics, Glycomics, and antigenicity. Wiley-Blackwell, Weinheim.
Takashi, T., Takumi, H., Takeo, M., Yuzo, K., Guo-Jun, Z., Takashi, F., Iwao, O., 2005. Hybridization of deoxyribonucleic acid and immobilization of green fluorescent protein on nanostructured organosilane templates. Jpn. J. Appl. Phys. 44 (7S), 5851.
Vafaei, S., Podowski, M.Z., 2005. Analysis of the relationship between liquid droplet size and contact angle. Adv. Colloid Interface Sci. 113 (2–3), 133–146.
Vasina, E.N., Paszek, E., Nicolau Jr, D.V., Nicolau, D.V., 2009. The BAD project: data mining, database and prediction of protein adsorption on surfaces. Lab a Chip 9 (7), 891–900.
Yunker, P.J., Still, T., Lohr, M.A., Yodh, A.G., 2011. Suppression of the coffee-ring effect by shape-dependent capillary interactions. Nature 476 (7360), 308–311.

Protein microarray spots are modulated by the patterning method, surface chemistry and processing conditions

Kathryn F.A. Clancy, Sebastien Dery, Veronique Laforte, Prasad, Shetty,
David Juncker, and Dan V. Nicolau

SUPPLEMENTARY INFORMATION

PART 1: ADDITIONAL TEXT

1. Glossary of terms

Coffee-ring ratio (CRR) is the ratio between the number of pixels found in the outer 50% of the spot vs. the number of pixels within the inner 50% of the spot. The boundaries of the inner 50% of the spot and the outer 50% of the spot are based on the distance from the centroid of the spot to the outer edge found after thresholding. A value of -1 represents the 'coffee-ring' morphology, where all of the pixels with an intensity above the background signal are in the outer 50% of the spot. A value of +1 represents the 'bull's eye' morphology, where all the pixels with intensity values greater than that of the background are found in the inner 50% of the spot. A value of 0 represents a perfectly even distribution of the fluorescent pixels within the spot.

Spot size regularity is defined as the ratio between the standard deviation from each triplicate measurement by its mean spot size, i.e., relative standard deviation = (standard deviation)/mean. It is used to quantify the regularity of spot size resulting from different printing methods.

Eccentricity is defined as the ratio of the distance between the center of a spot and its major axis length, is a measure used to quantify the deviation of a spot from a perfect circle. An eccentricity value of zero represents a perfect circle with a constant radius around the central axis, and a value of one represents a line. The eccentricity can be used to quantify the regularity of the shape of the deposited pattern from spot to spot. Usually, the segmentation of spots from the background signal is performed using a grid system. This technique uses the size of the spots to estimate spot spacing then transposes this information to find other spots on the array. If the spots are not circular, and an automatic grid system is being used for segmentation, the eccentric circles may fall outside the expected geometric parameters and cause errors in signal quantification. Additionally, in other quantification approaches, the spots are assumed circular and measurements are based on the signal within a predefined circle.

2. Full description of Materials and Methods

Reagents. A 1X (0.01M) phosphate buffered saline (PBS) solution of pH 7.4 was prepared in MilliQ water and used as a diluent for all printing methods, i.e., micro-contact printing (μCP), inkjet printing, and pin printing. A 1X PBS solution with previously optimized additives (25% 2,3-butanediol/2M betaine, herein shortened PBSbb), which limits droplet evaporation, maximizes immunoassay binding signal, and gives a favourable spot morphology (Bergeron et al. 2015).

Proteins. Purified fluorophore conjugated IgG (Cy5® Goat Anti-Rabbit IgG (H+L), from Life Technologies), and fluorophore conjugated BSA (Alexa Fluor® 647, from Molecular Probes) have been used for protein labelling. The molecular weight and pI of IgG and BSA are 150-170 kDa, and 66 kDa, respectively, and their pIs are 7.3 ±1.2, and 4.65, respectively.

Surface modification chemistry. Prior to modification, glass slides (Fisherfinist, Fisher Scientific) were cleaned by sonication in 100% ethanol for a minimum of 10 minutes, dried with N_2, then plasma treated for 2 minutes. The cleaned slides were then modified by deposition of silanes with various terminal functional groups. 3-Glycidoxypropyl-dimethoxymethyl silane (GPS), Trichloro(octyl) silane (OTS), and 3-(Aminopropyl)-triethoxy silane (APTES) slides were

prepared by liquid deposition as described elsewhere (Huang et al. 2003; Karrasch et al. 1993; Nam et al. 2006). Trichloro(1H,1H,2H,2H-perfluorooctyl) silane (PFS) slides were prepared by chemical vapour deposition within a dessicator at room temperature for minimum 4 hours[1] (Huang et al. 2003; Kim et al. 2011). After surface modification, all slides were kept away from sunlight in a dust-free box that was enclosed within a bag filled with N_2 for a maximum of one week before use.

Contact Angle Measurements. Advancing and receding contact angles were measured using 3 µl double distilled water droplets, and a contact angle goniometer with video capability (OCA 15 EC, Dataphysics).

Inkjet Printing. A non-contact piezo-microarrayer (Nanoplotter 2.0, GeSiM) with a single nozzle was used to deposit 0.4 nL of protein solution on target surfaces to create 8x8 arrays with a pitch of 200 µm between spots, for a total of 16 spots per concentration, per replicate slide (Supplementary Figure SI 1). All printing was performed at room temperature and 65% humidity. After printing, the surfaces were kept in humidified conditions for 2 hours incubation before rinsing. Rinsing of the whole substrate surface was performed for 10 seconds either with a 1XPBS solution or a 1XPBS solution with 0.1% Tween-20 (PBST), then rinsed 10 seconds with MilliQ water and dried with N_2 gas. A PBST wash is a standard wash in microarray research, whereas PBS is a much milder. The use of the latter wash enables the demonstration of how the PBST wash increases printed spot uniformity.

Pin Printing. Contact pin printing was carried out with a customized Nanoplotter 2.1 microarrayer (GeSiM) equipped with a silicon contact printing head and precision microfabricated collimator (Parallel Synthesis, Santa Clara, CA). The printer contains a tailored slide tray with spring-loaded clamps for each individual slide (GeSiM). Four silicon quill pins were used simultaneously to create 5x5 arrays of replicate 63-74 pL spots (volume delivered depended on hydrophobicity of surface) with a pitch of 200 µm and with a contact time of 0.1 second onto target surfaces for a total of 100 spots per concentration per replicate slide (Supplementary Figure SI 1). All subsequent printing parameters and steps were performed the same as done with inkjet printing.

Microcontact Printing (µCP). A patterned silicon wafer was used to fabricate flat, 15 µm-wide square stamps with a pitch of 75 µm between square posts. Poly(dimethylsiloxane) (PDMS) stamps were created as previously described (Ricoult et al. 2014)(details in the Supplementary Information section I). The stamps were cleaned before use by ultrasonication in 70% ethanol, for a minimum of 5 minutes, and dried under a stream of N_2 gas. After drying, the patterned side of the stamp was inked with 10 µl of the fluorophore conjugated protein solution underneath a plasma-activated coverslip for 5 minutes. The coverslip was then removed, the stamps rinsed with 1X PBS and MilliQ water each for 10 seconds then rapidly dried under a stream of N_2. Immediately after, the inked, patterned side of the stamp was placed on the desired surface, and a 25 mg weight placed on top for 5 seconds and then weight and stamp were lifted off sequentially at a 90° angle (Ricoult et al. 2014).

Image Acquisition and Analysis. Fluorescent images were obtained using an Agilent G2565CA microarray scanner system at 30% laser power using the red filter at a 2 µm x 2 µm resolution. A custom Matlab script was written for image analysis and quantification. (MATLAB 2015). Automatic determination of an adequate threshold to distinguish the background fluorescence from the protein deposition pattern is a difficult challenge (Draghici 2003). In this work, an

optimization approach was used, consisting on iteratively narrowing down on an optimal threshold value corresponding to a minimal sum of errors fit regarding the expected Gaussian curve of the fluorescent signal. An additional size constraint on the expected spot size was added for quality control. Measurements at each deposition spot were then performed and stored for further analysis along with images of the thresholded map for visual inspection.

The edge of a single spot was defined by a pixel where no adjacent pixels contained a fluorescence signal above the threshold. The spot size was determined by adding all of the pixels up within a spot then multiplying this value by 4 (2 μm x 2 μm) to give the spot size in μm^2. Eccentricity of the spot was calculated by finding the ratio of the distance between the foci of the spot and its major axis length. All the aforementioned analysis was performed using the *regionprops* image analysis function in Matlab.

The cross-section of the mean fluorescence signal across a printed spot was quantified by tracing a line of the fluorescence across the spot through the centroid, and extending the line by an equal distance in opposite directions from the centroid. The uniformity of the fluorescence signal across a spot was quantified by computing a coffee-ring ratio.

The raw image files were first segmented based on predefined search areas, then automatic thresholding was performed. The spots outside of the expected area were eliminated. Each individual spot was then analysed.

Statistical Analysis. Error bars in all figures represent the standard error. Technical replicates were grouped for statistical analysis and determination of significance was performed using the Student's t-test in Matlab.

References

Bergeron, S., Laforte, V., Lo, P.S., Li, H., Juncker, D., 2015. Evaluating mixtures of 14 hygroscopic additives to improve antibody microarray performance. Anal Bioanal Chem 407(28), 8451-8462.

Draghici, S., Lenhart, S., Safer, H., Maini, P., Etheridge, A., Gross, L. , 2003. Data Analysis Tools for DNA Microarrays. New York: Chapman and Hall/CRC.

Huang, T.T., Sturgis, J., Gomez, R., Geng, T., Bashir, R., Bhunia, A.K., Robinson, J.P., Ladisch, M.R., 2003. Composite surface for blocking bacterial adsorption on protein biochips. Biotechnol Bioeng 81(5), 618-624.

Karrasch, S., Dolder, M., Schabert, F., Ramsden, J., Engel, A., 1993. Covalent binding of biological samples to solid supports for scanning probe microscopy in buffer solution. Biophys J 65(6), 2437-2446.

Kim, D.J., Lee, J.M., Park, J.G., Chung, B.G., 2011. A self-assembled monolayer-based micropatterned array for controlling cell adhesion and protein adsorption. Biotechnol Bioeng 108(5), 1194-1202.

MATLAB, 2015. vol. 2015b, 8.6.0.267246 ed. Natick, Massachusetts: The MathWorks Inc.

Nam, Y., Branch, D.W., Wheeler, B.C., 2006. Epoxy-silane linking of biomolecules is simple and effective for patterning neuronal cultures. Biosens Bioelectron 22(5), 589-597.

Ricoult, S.G., Nezhad, A.S., Knapp-Mohammady, M., Kennedy, T.E., Juncker, D., 2014. Humidified microcontact printing of proteins: universal patterning of proteins on both low and high energy surfaces. Langmuir 30(40), 12002-12010.

Protein microarray spots are modulated by the patterning method, surface chemistry and processing conditions

Kathryn F.A. Clancy, Sebastien Dery, Veronique Laforte, Prasad, Shetty,
David Juncker, and Dan V. Nicolau

SUPPLEMENTARY INFORMATION

PART 2: ADDITIONAL FIGURES

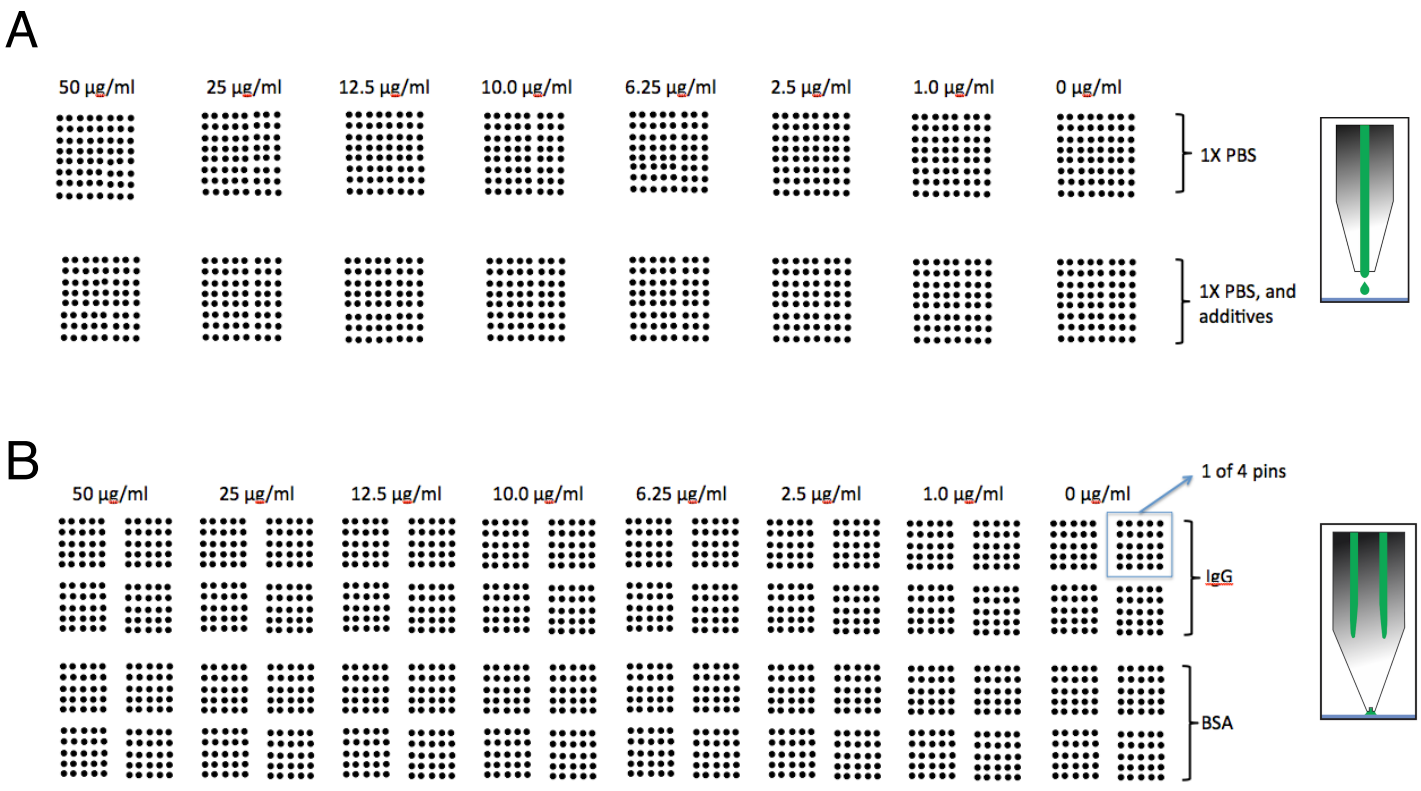

Supplementary Figure S1. Schematics of the Inkjet printing layout (A) and Pin printing layout (B) used during experiments.

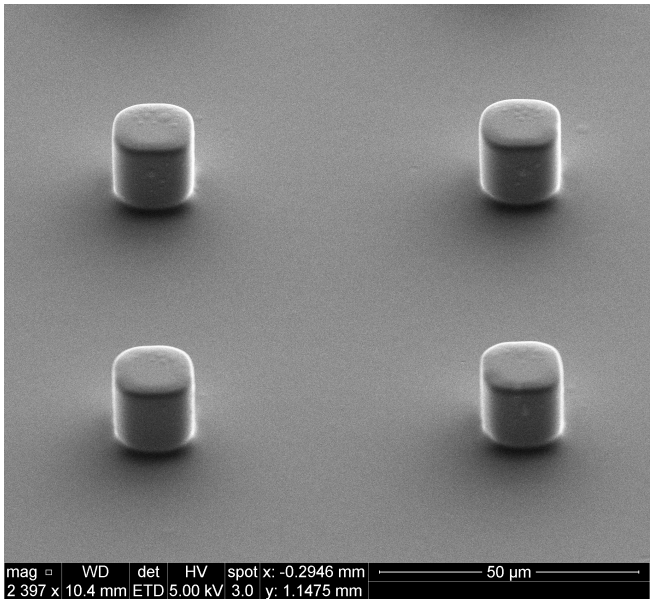

Supplementary Figure S2. Electron microscopy image of the polydimethoxysilane (PDMS) stamps used during experiments.

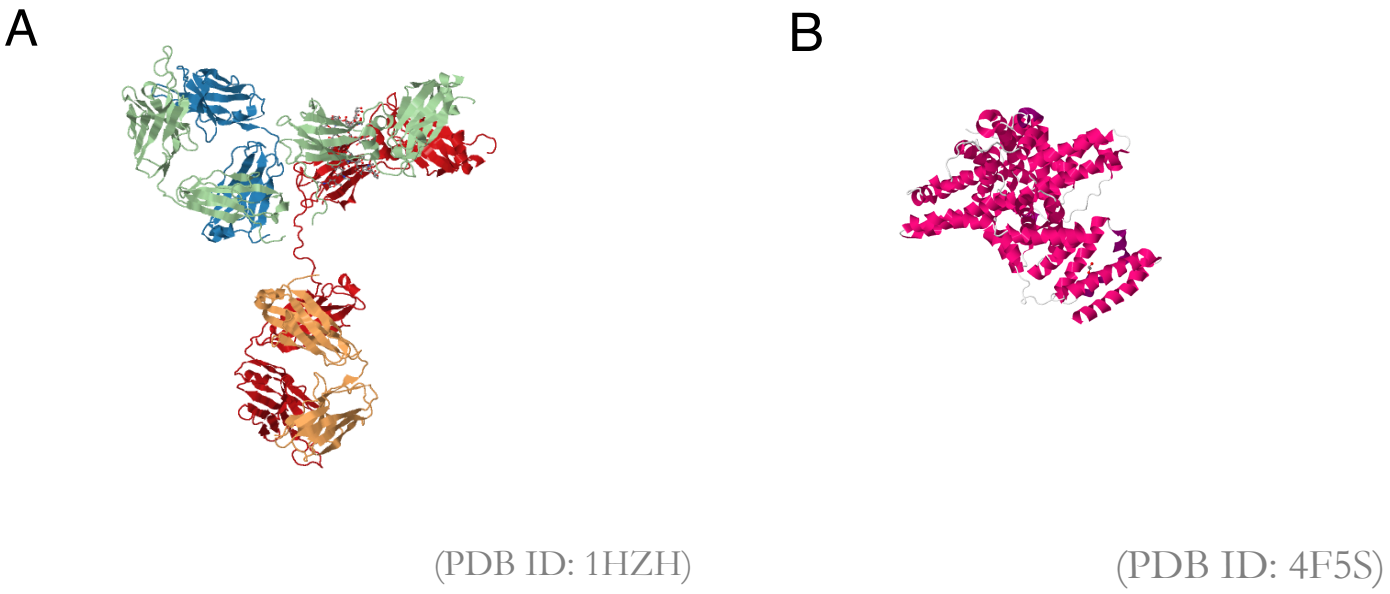

Supplementary Figure S3. Representative ribbon models of the IgG (A) and BSA (B) proteins used for microarray experiments from the Protein Data Bank (https://www.rcsb.org/).

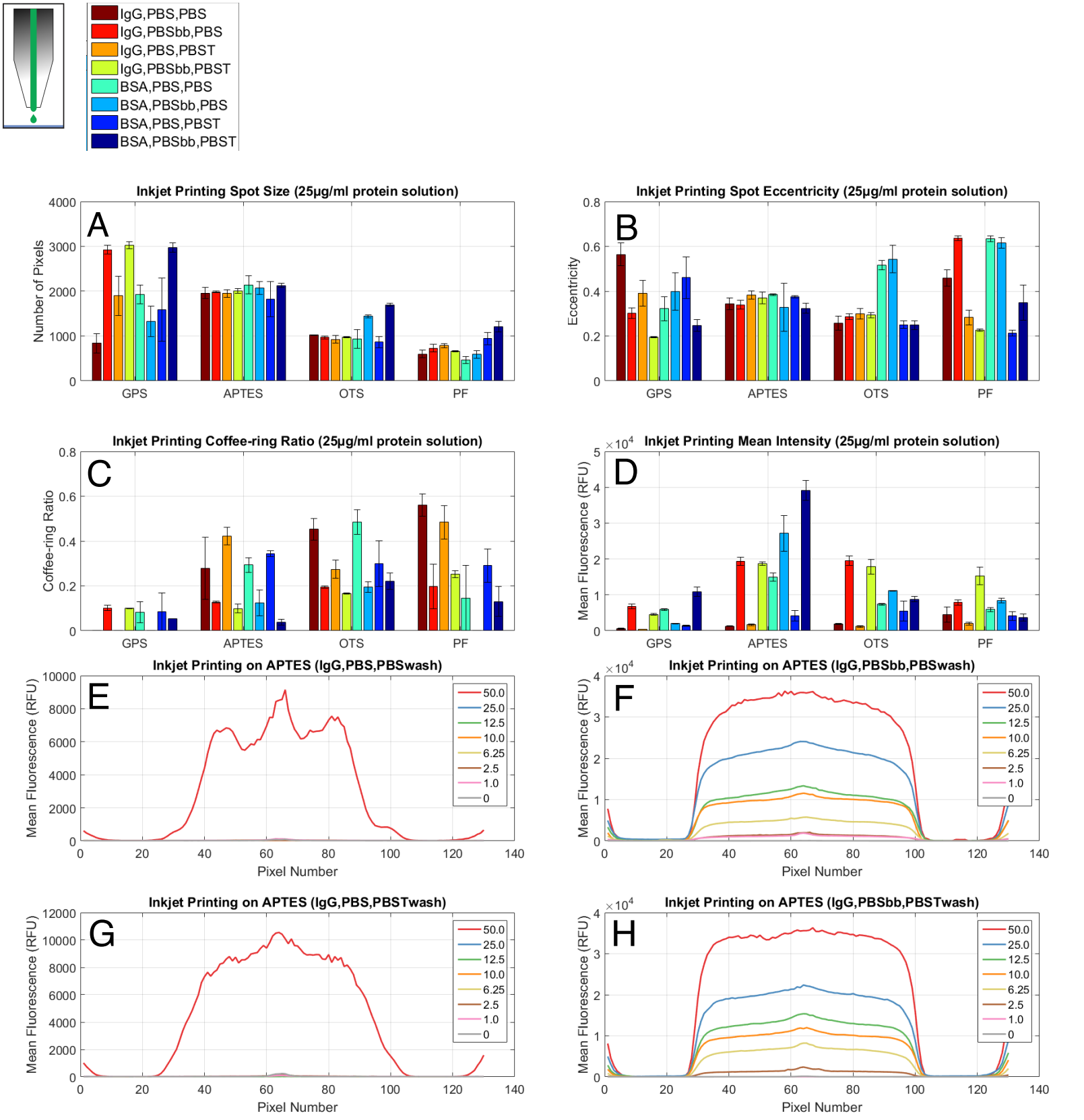

Supplementary Figure S4. Effect of buffer and washing conditions when deposit a 25 μg/ml protein solution by inkjet printing onto GPS-, APTES-, OTS-, and PFS-functionalized glass slides on the spot size (A), eccentricity (B), coffee-ring ratio (C), and mean fluorescence intensity (D). Protein solutions were suspended in either a phosphate buffered saline (PBS) solution of pH 7.4 or a PBS with 25% 2,3-butandiol/2M betaine (PBSbb). Following printing, slides were rinsed for 10 seconds with either a 1X PBS or a 1XPBS solution with 0.1% Tween-20 (PBST) and then rinsed 10 seconds with MilliQ water and dried with N_2 gas. The difference in the fluorescence profile of IgG spots: suspended in PBS and washed with PBS (E); suspended in PBSbb and washed with PBS (F); suspended in PBS and washed with PBST (G); and suspended in PBSbb and washed with PBST (H).

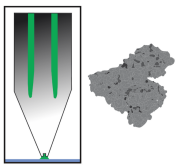

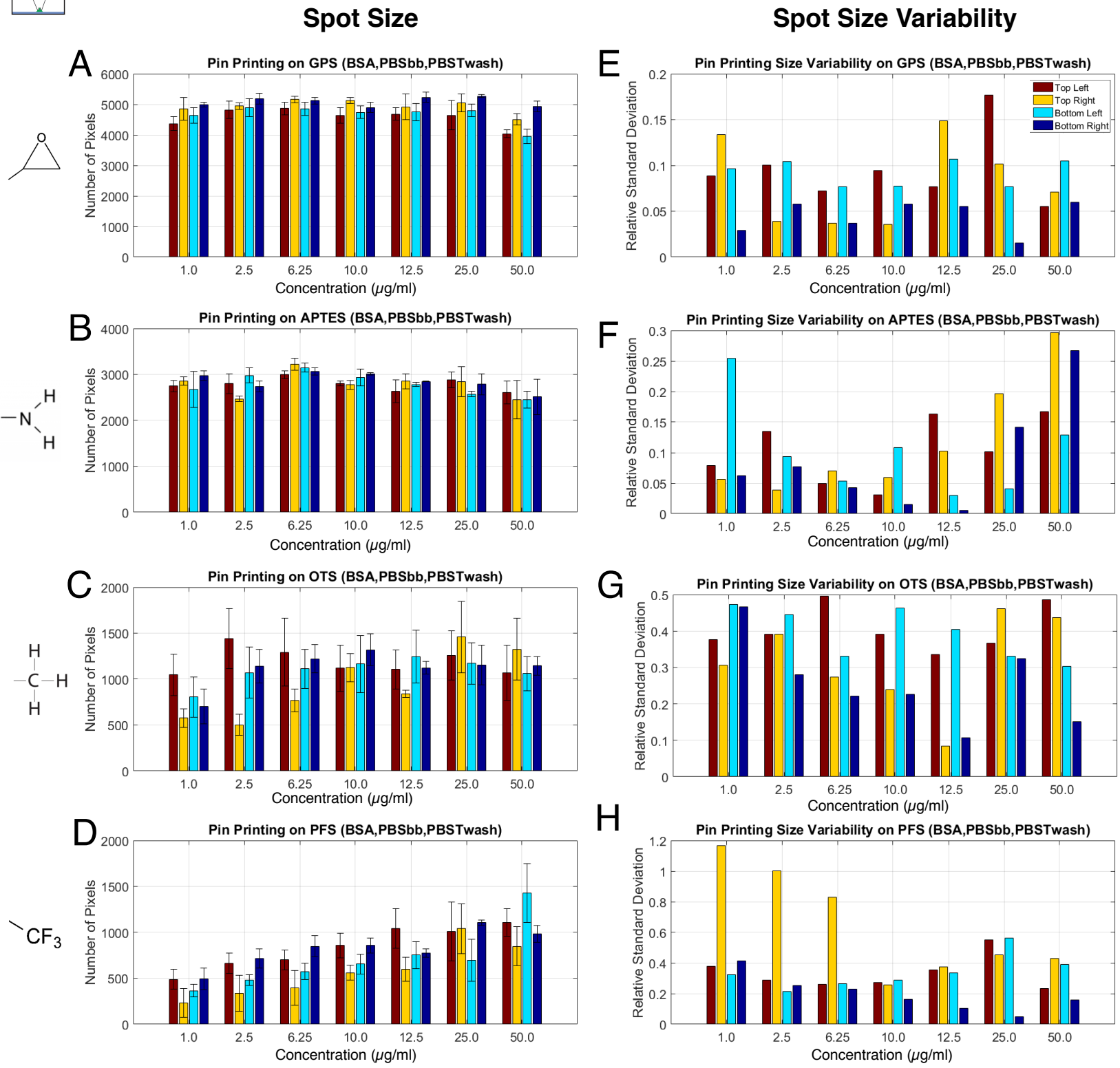

Supplementary Figure S5. Analysis of results from each individual nozzle used during the pin printing of BSA onto GPS- (A,E), APTES- (B,F), OTS- (C,G), and PFS-functionalized (D,H) glass slides on the spot size (A-D) and spot size variability (E-H).

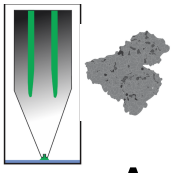

Eccentricity

Coffee-ring Ratio

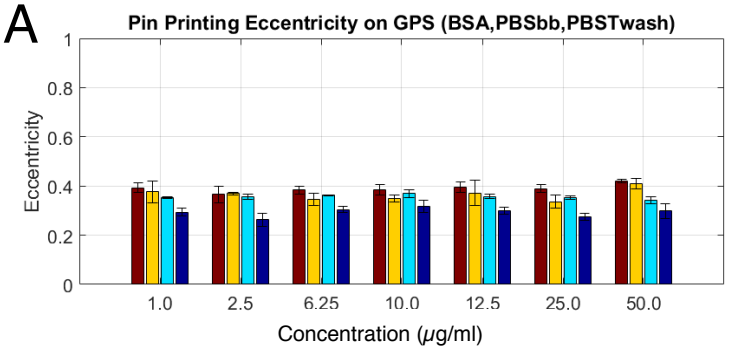

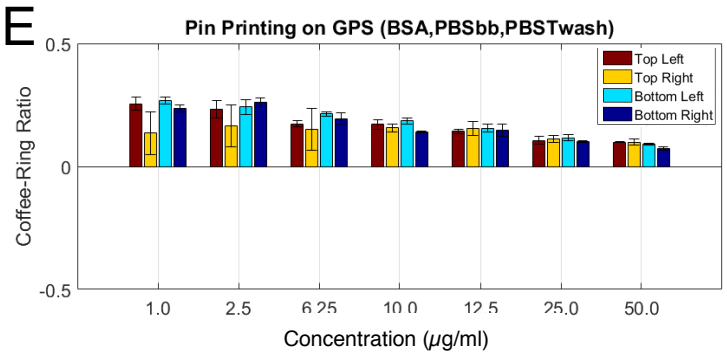

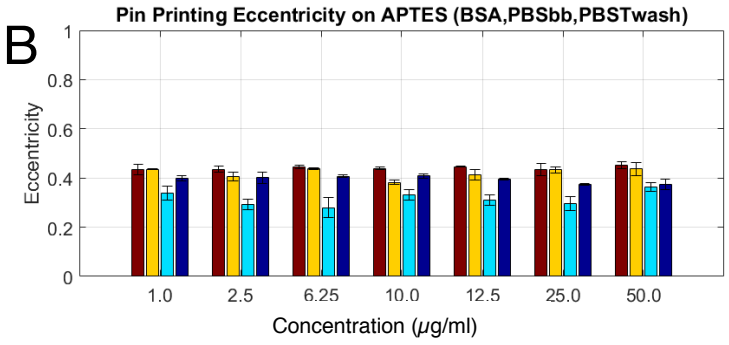

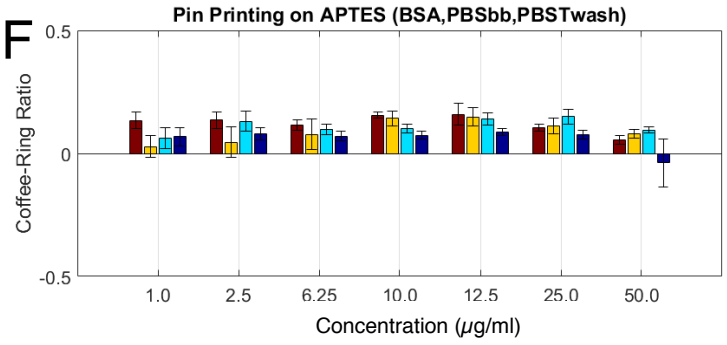

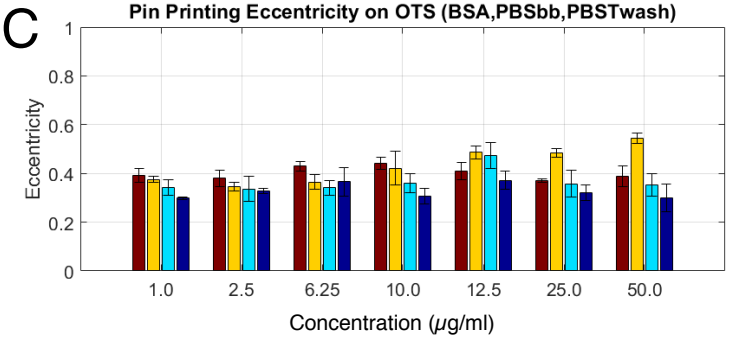

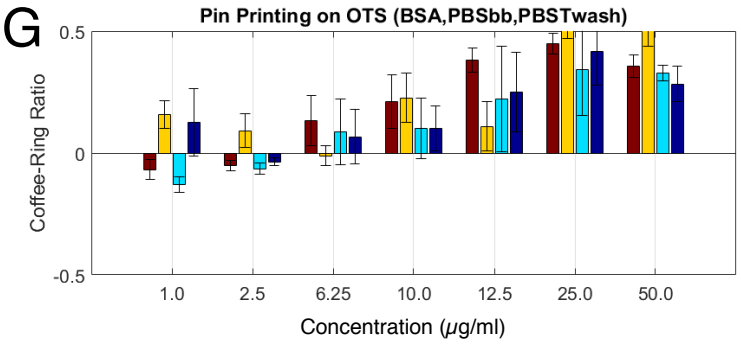

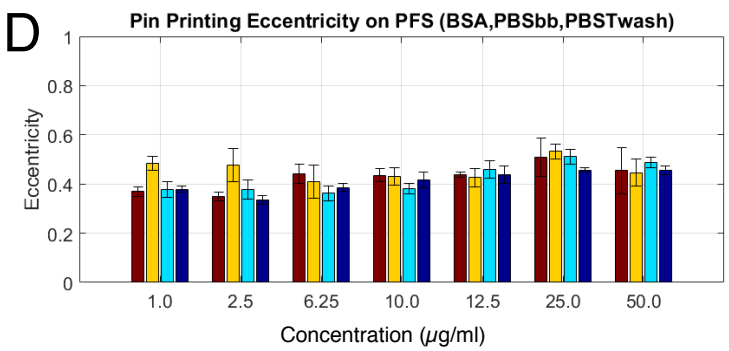

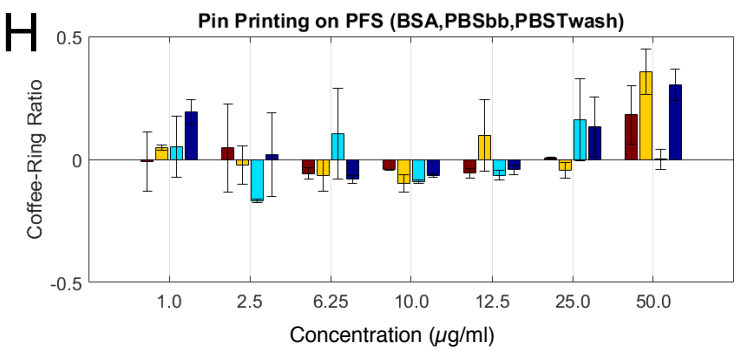

Supplementary Figure S6. Analysis of results from each individual nozzle used during the pin printing of BSA onto GPS- (A,E), APTES- (B,F), OTS- (C,G), and PFS-functionalized (D,H) glass slides on the spot eccentricity (A-D) and the calculated coffee-ring ratio (E-H).

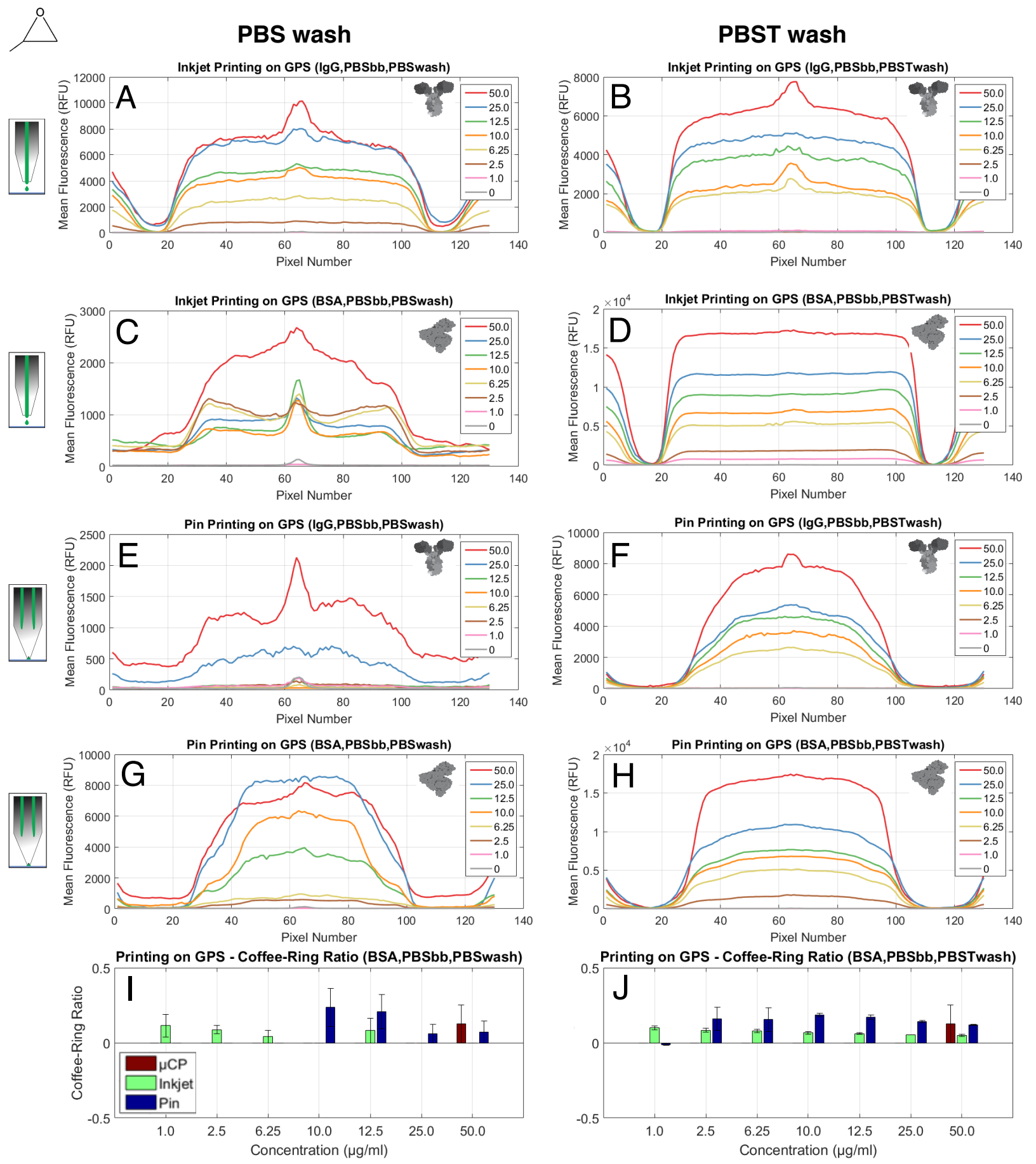

Supplementary Figure S7. Fluorescence intensity profile of IgG (A,B,E,F) and BSA (C,D,G,H) spots printed by inkjet (A-D) and pin printing (E-H) onto GPS functionalized slides then washed with either PBS (left) or PBST (right) and the resulting coffee-ring ratio for BSA (I,J) of varying concentration (0, 1.0, 2.5, 6.25, 10.0, 12.5, 25.0, and 50.0 μg/ml).

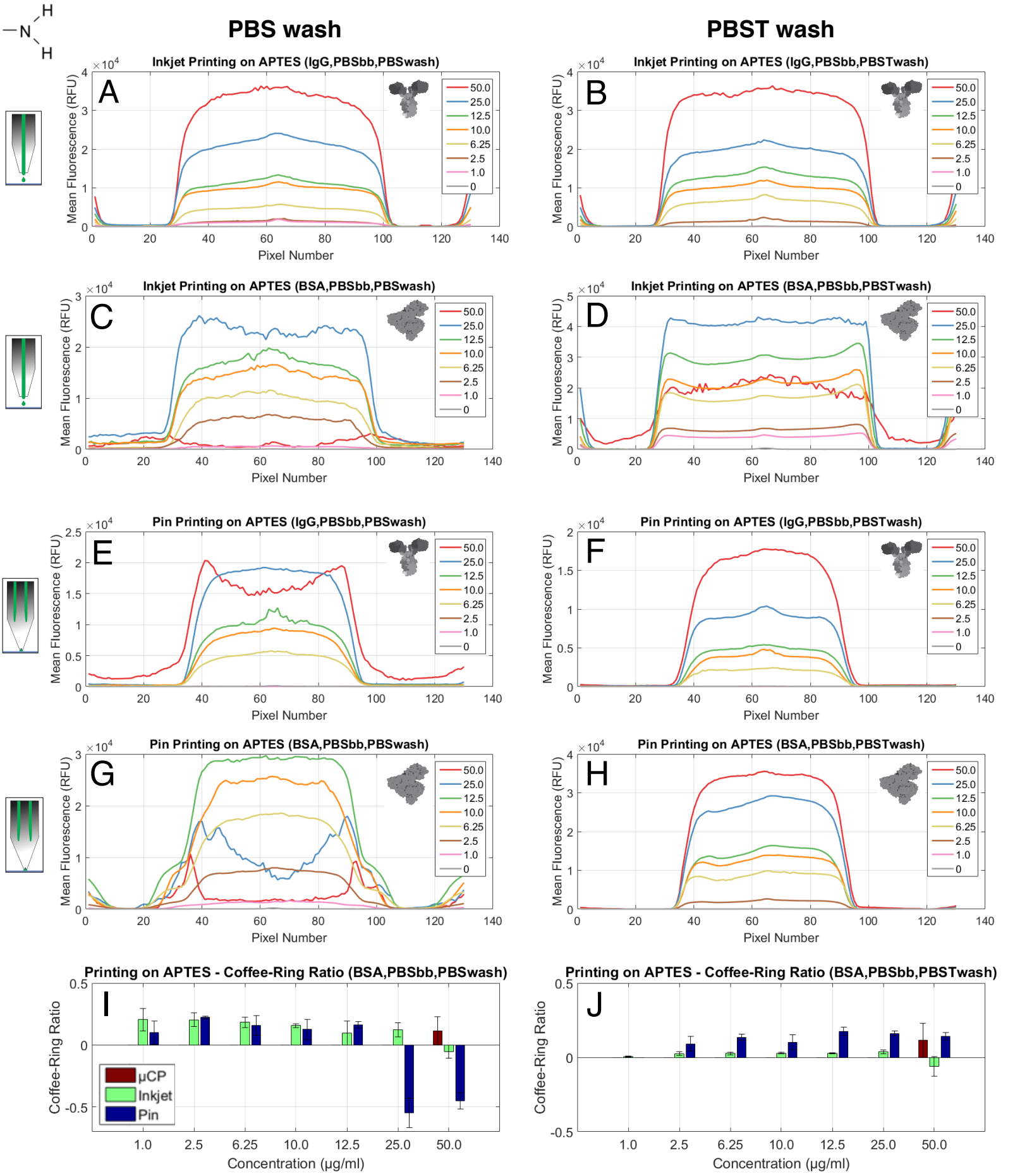

Supplementary Figure S8. Fluorescence intensity profile of IgG (A,B,E,F) and BSA (C,D,G,H) spots printed by inkjet (A-D) and pin printing (E-H) onto APTES slides then washed with either PBS (left) or PBST (right) and the resulting coffee-ring ratio for BSA (I,J) of varying concentration (0, 1.0, 2.5, 6.25, 10.0, 12.5, 25.0, and 50.0 μg/ml).

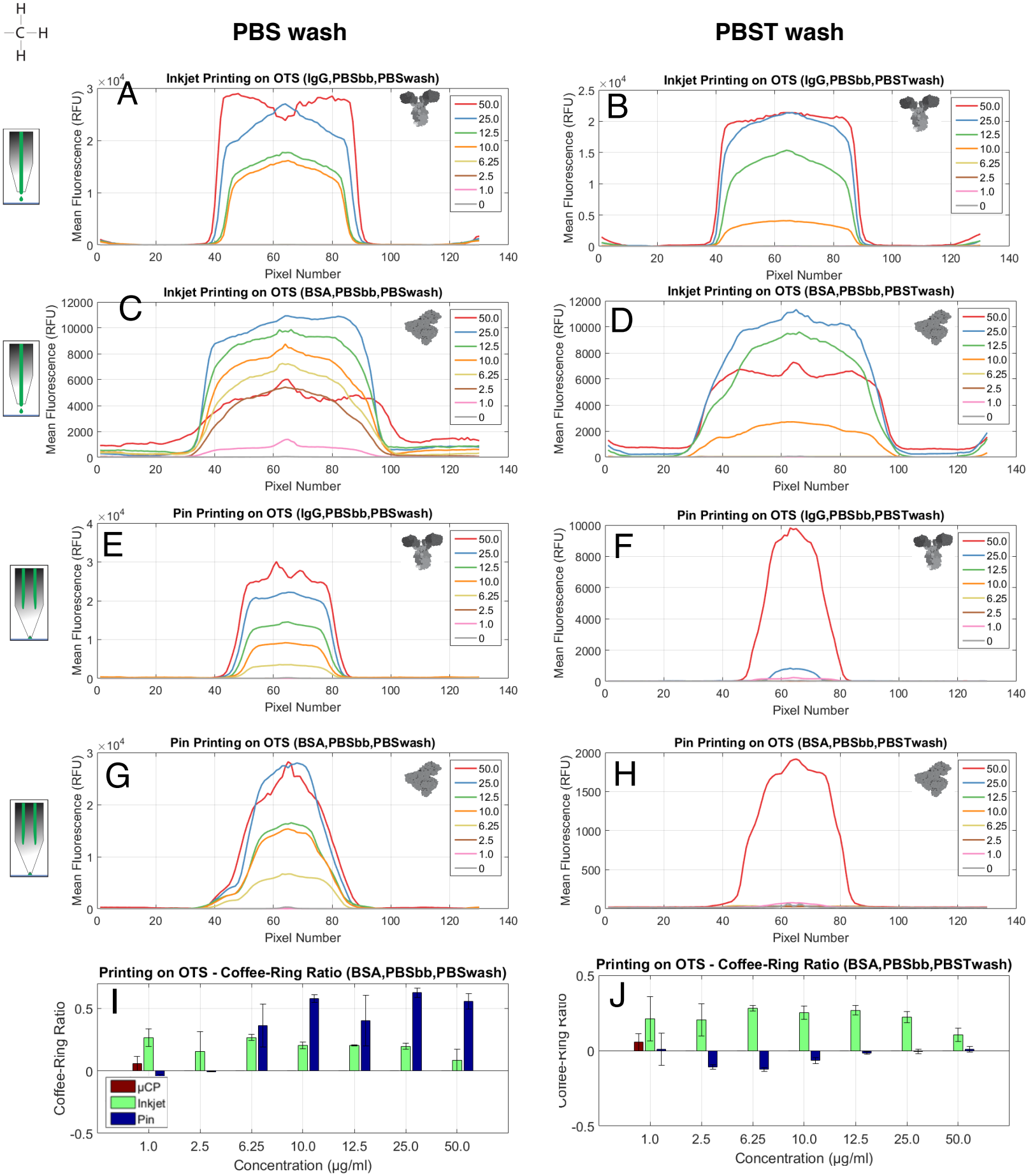

Supplementary Figure S9. Fluorescence intensity profile of IgG (A,B,E,F) and BSA (C,D,G,H) spots printed by inkjet (A-D) and pin printing (E-H) onto OTS functionalized slides then washed with either PBS (left) or PBST (right) and the resulting coffee-ring ratio for BSA (I,J) of varying concentration (0, 1.0, 2.5, 6.25, 10.0, 12.5, 25.0, and 50.0 μg/ml).

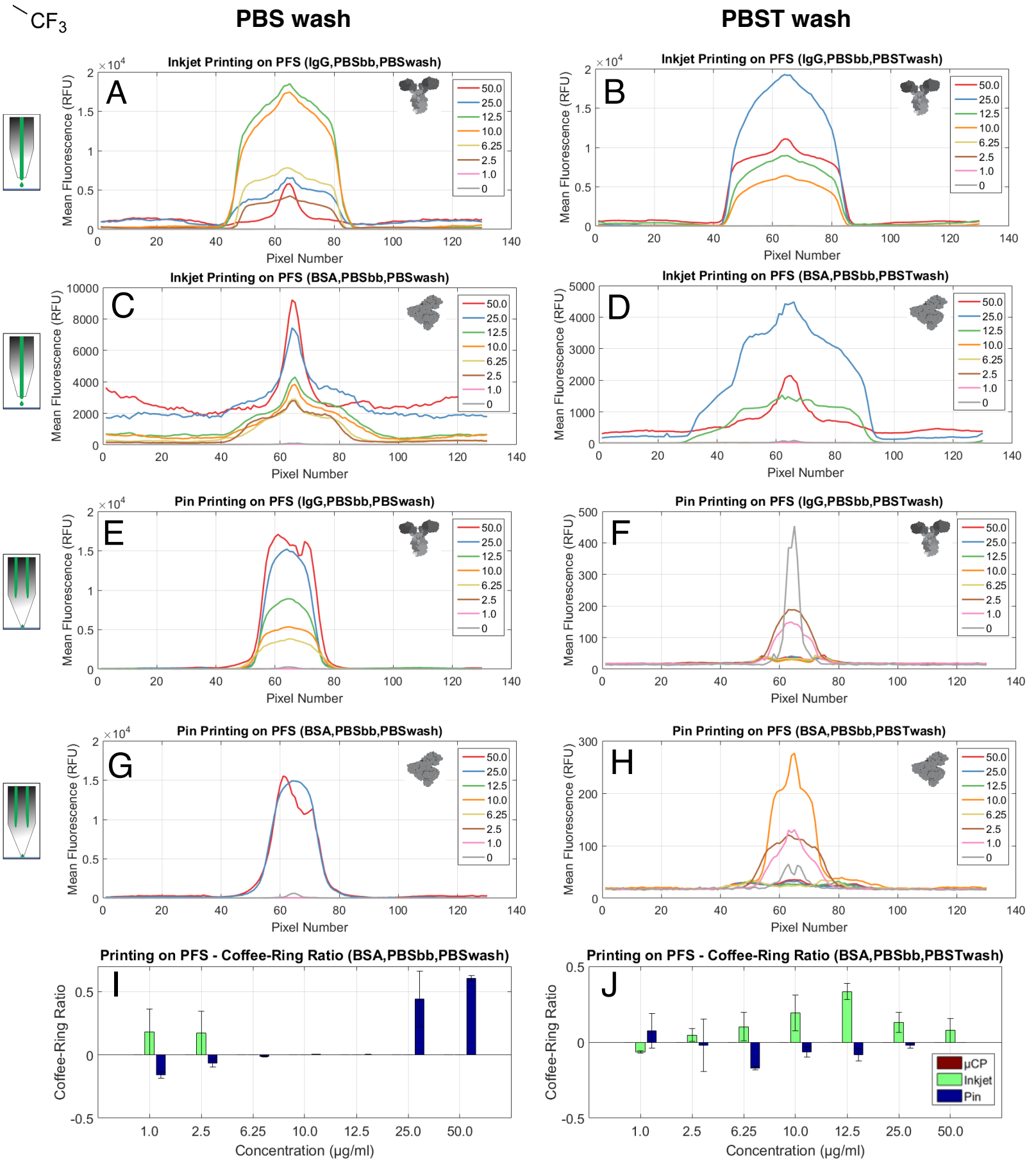

Supplementary Figure S10. Fluorescence intensity profile of IgG (A,B,E,F) and BSA (C,D,G,H) spots printed by inkjet (A-D) and pin printing (E-H) onto PFS functionalized slides then washed with either PBS (left) or PBST (right) and the resulting coffee-ring ratio for BSA (I,J) of varying concentration (0, 1.0, 2.5, 6.25, 10.0, 12.5, 25.0, and 50.0 μg/ml).

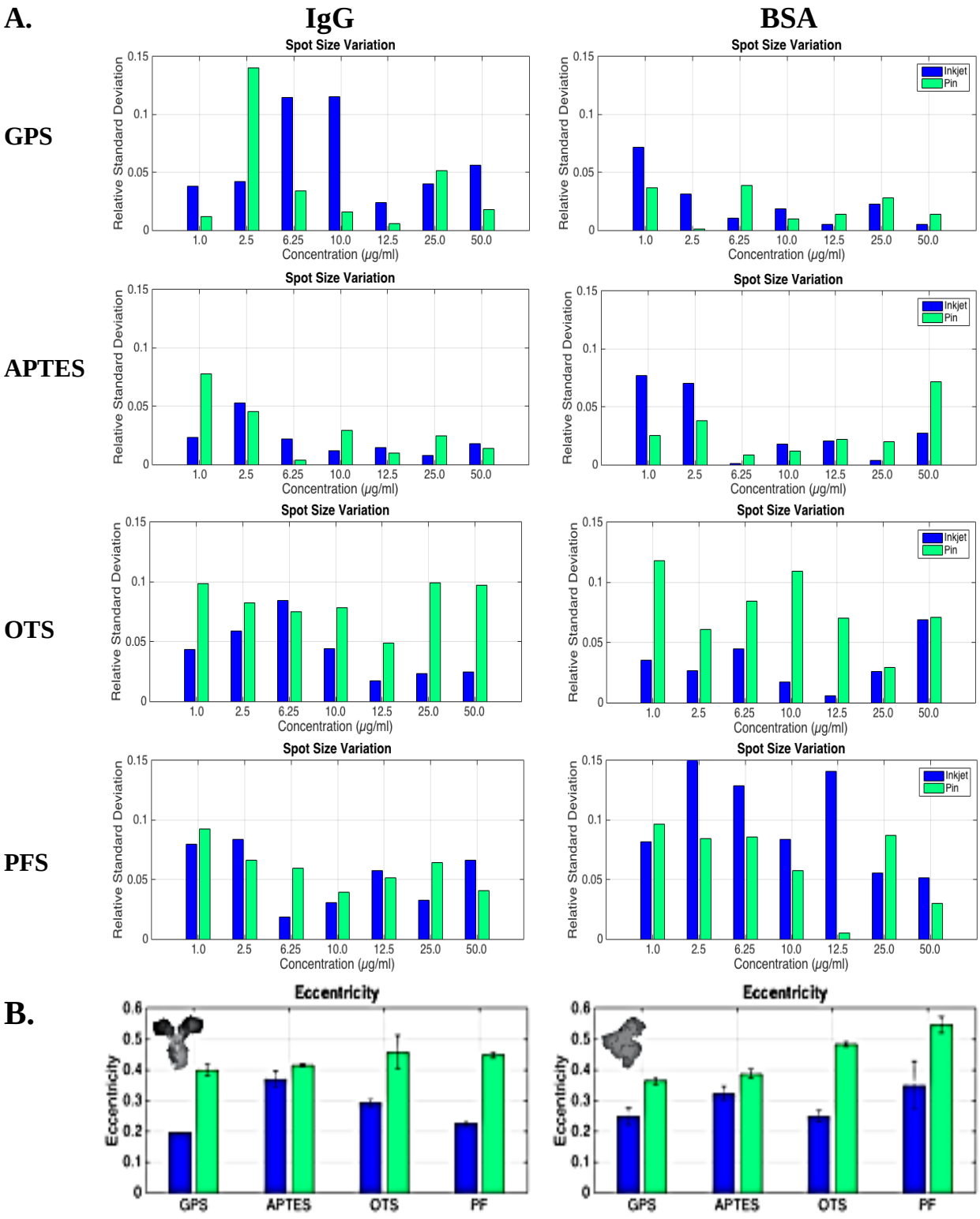

Supplementary Figure S11. Spot size variability and morphology. (A) Variability: relative standard deviation of spot size from inkjet (blue), and pin (green) printing for IgG or BSA solutions (1.0-50 µg/ml) on silane-functionalized glass slides. (B) Eccentricity of spots produced by inkjet and pin printing on silane-functionalized glass of increasing hydrophobicity. Left: IgG; reight: BSA. Error bars represent standard errors.

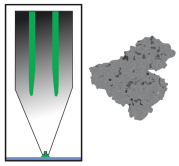

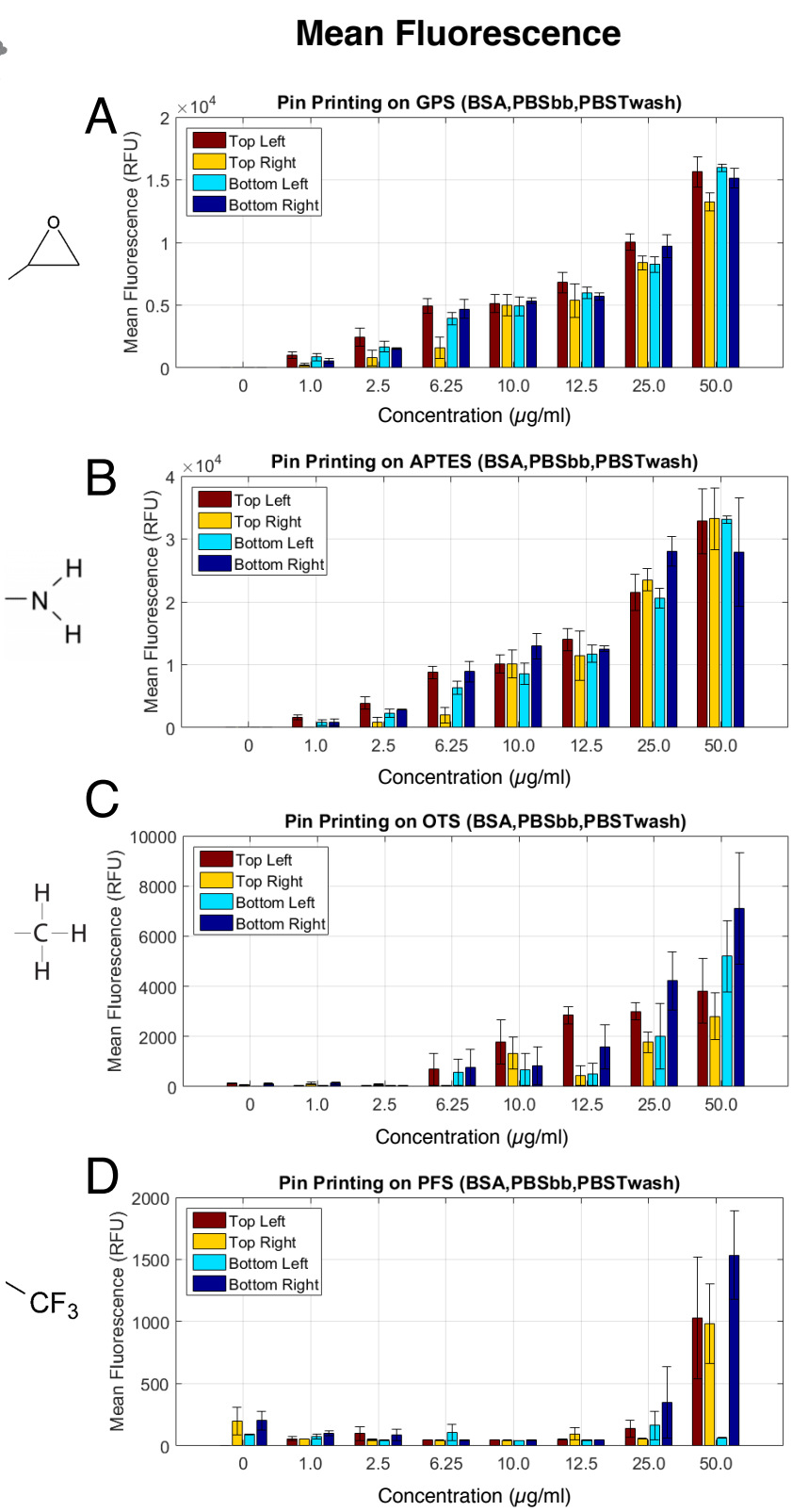

Supplementary Figure S12. Analysis of results from each individual nozzle used during the pin printing of BSA onto GPS- (A), APTES- (B), OTS- (C), and PFS-functionalized (D) glass slides on the spot mean fluorescence intensity.

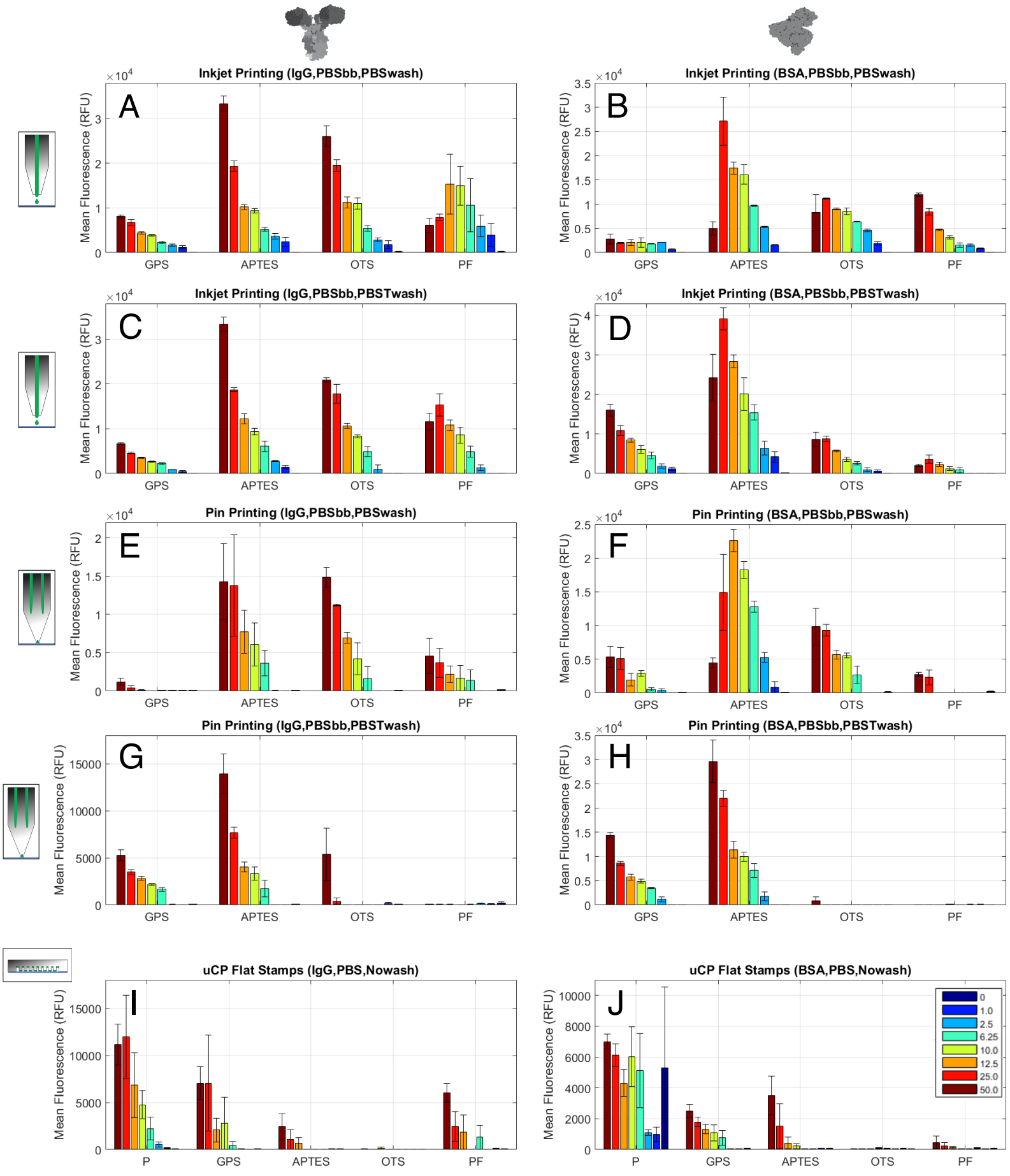

Supplementary Figure S13. Mean fluorescence intensity of IgG (left) and BSA (right) spots printed by inkjet (A-D), pin (E-H), and microcontact printing (μCP) (I-J) onto GPS-, APTES-, OTS-, PFS-functionalized, and Plasma (P, only μCP) glass slides of varying concentration (0, 1.0, 2.5, 6.25, 10.0, 12.5, 25.0, and 50.0 μg/ml).

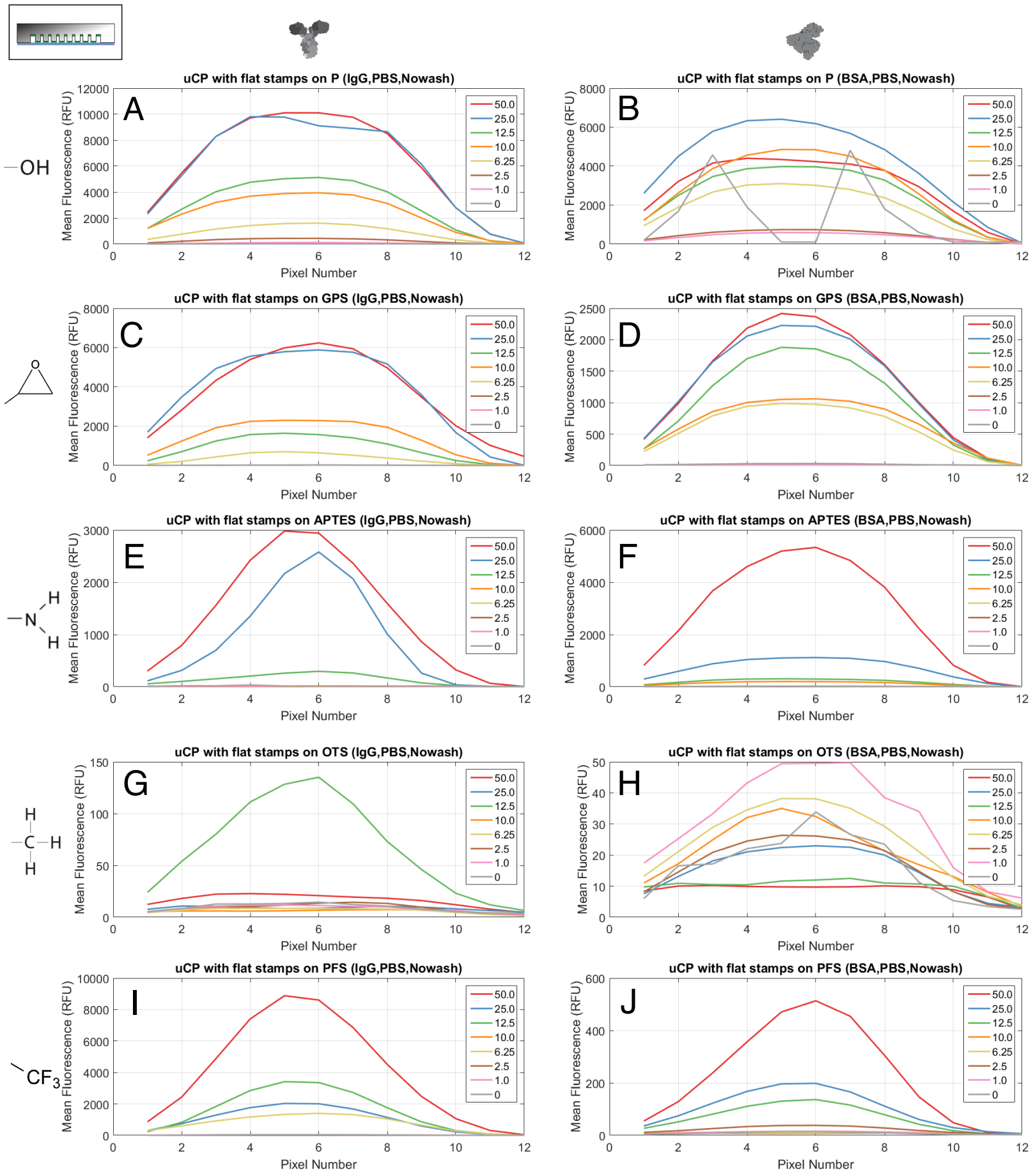

Supplementary Figure S14. Fluorescence intensity profile of IgG (left) and BSA (right) spots printed by microcontact printing onto Plasma (A,B), GPS- (C,D), APTES- (E,F), OTS- (G,H), and PFS-functionalized (I,J) glass slides.